Testbeam Experiments
and
Monte Carlo Simulation
of the
ZEUS 6m Tagger

Diplomarbeit
Fachbereich Physik
Universität Hamburg

Nils Krumnack

Hamburg, July 2001

Abstract

The electron/proton collider HERA has upgraded its luminosity in 2000/2001 requiring the ZEUS luminosity monitoring system to be upgraded to. Subject of this diploma thesis is the experimental test of the 6m tagger, which is part of this new system.

The 6m tagger is a tungsten/scintillator spaghetti calorimeter. It will be installed about 6 m away from the interaction point inside a quadrupole magnet. Therefore it has to be of very compact size (85×23 mm^2).

Despite its small size it has an energy resolution of $16\%/\sqrt{E/\,\mathrm{GeV}}$ and at 5 GeV a position resolution of 0.93 mm in x- and 0.51 mm in y-direction.

Kurzfassung

Der Elektronen-Protonen-Beschleuniger HERA hat seine Luminosität in 2000/2001 erhöht, was große Änderungen am ZEUS-Luminositätsmesssystem erforderlich machte. Thema dieser Arbeit ist die experimentelle Untersuchung des 6m-Taggers, welcher Teil des neuen Systems ist.

Der 6m-Tagger ist ein Wolfram-Szintillator-Spaghetti-Kalorimeter. Er wird ungefähr 6 m vom Wechselwirkungspunkt entfernt in einem Quadropolmagneten installiert. Deswegen muss er sehr klein sein (85×23 mm^2).

Trotz seiner geringen Größe hat er eine Energieauflösung von $16\%/\sqrt{E/\,\mathrm{GeV}}$ und bei 5 GeV eine Ortsauflösung von 0.93 mm in x- und 0.51 mm in y-Richtung.

Contents

1 Introduction **1**

2 The ZEUS detector **3**
2.1 HERA and ZEUS 3
2.2 The ZEUS luminosity measurement system 4
2.3 The 6m tagger 5

3 Detector description **7**
3.1 Detector geometry 7
3.2 Monte Carlo Simulation 10
3.3 The EGS4 package 12

4 Reconstruction Algorithms **13**
4.1 Reconstruction regions 13
4.2 Energy reconstruction 14
4.3 Position reconstruction 15
4.3.1 Basic reconstruction 15
4.3.2 Corrected reconstruction 15

5 Prototype measurements **17**
5.1 Testbeam setup 17
5.2 Calibration 18
5.3 Energy scan 20
5.4 Fine scan 23
5.5 Summary of testbeam measurement 27

6 Measurements with the complete detector **29**
6.1 Testbeam setup 29
6.2 Calibration 30
6.3 Energy scan 30
6.4 Fine scan 33
6.5 Influence of incident angle 37
6.6 Gate length study 37
6.7 Summary of testbeam measurements 37

7 Summary **41**

A Calibration data **43**

B Software documentation **53**
B.1 The Monte Carlo simulation 53
B.2 The treebuilder program 54
B.3 The analysis program 58

Bibliography **61**

Index **63**

Chapter 1

Introduction

HERA is an electron/proton collider located at DESY, Germany. Electrons or positrons of 27.5 GeV collide with protons of 920 GeV. The ZEUS detector is a large, general purpose detector situated in the South Hall of the HERA accelerator.

In 2000/2001 a luminosity upgrade was done at HERA. After the upgrade synchroton radiation and event rates will increase making major changes in the ZEUS luminosity monitoring system necessary. A new system consisting of three detectors, the photon calorimeter, the pair spectrometer and the 6m tagger, has been built.

The 6m tagger will be installed inside a HERA quadrupole magnet. At this position it is subject to high temperatures, high radiation and severe space constraints. Still it must provide an energy resolution of about $15\%/\sqrt{E/\mathrm{GeV}}$ and a position resolution of less than 1 mm.

The assignments for this thesis were the development of a Monte Carlo simulation, testbeam measurements and their analysis and the development/ improvement of calibration/reconstruction algorithms.

This thesis is organized as follows: In the second chapter a general overview of ZEUS and the luminosity system is given, and in the third chapter a more detailed description of the 6m tagger. In the fourth chapter the different reconstruction algorithms are described. In the fifth and sixth chapter the results of the simulation and the measurements at the DESY testbeam for the prototype and final detector are presented.

Chapter 2

The ZEUS detector

2.1 HERA and ZEUS

At DESY (Deutsches Elektronen Synchroton) the worlds first electron-proton collider HERA (Hadron Elektron Ring Anlage) has been built. Four experiments are located at HERA: The two fixed target experiments HERMES and HERA-B and the two colliding experiments H1 and ZEUS. The ZEUS detector can be seen in figure 2.1 [Ze93a].

First electron-proton collisions were observed in 1991, physics operation started in 1992. In 2000, HERA was shut down for a luminosity upgrade which will yield in a highly increased luminosity when HERA starts again in 2001.

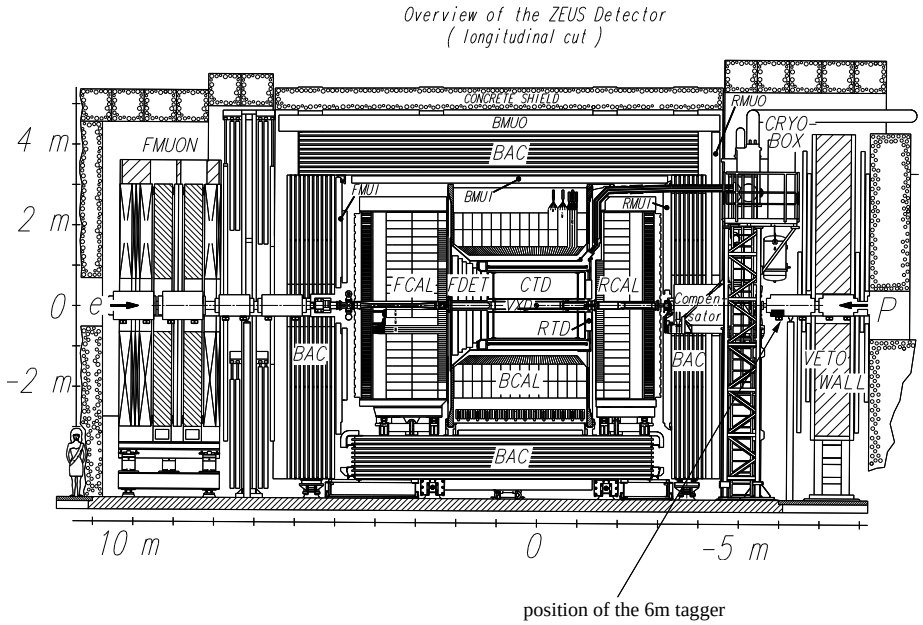

Figure 2.1: *The ZEUS detector. The planned position of the 6m tagger is marked.*

2.2 The ZEUS luminosity measurement system

To measure the cross section of a process one needs to measure the event rate of that process and the luminosity. The luminosity itself can be measured by measuring the event rate of a well known process with a reasonably high event rate.

The ZEUS luminosity measurement system (LUMI) works by measuring the well-known Bethe-Heitler Bremsstrahlung process [Be34a]

$$ep \rightarrow ep\gamma \tag{2.1}$$

The cross section of this process can be calculated with an accuracy of 0.5 % [Ga89a].

The old LUMI system used before the luminosity upgrade consisted of two detectors a photon detector 104 m from interaction point and an electron detector 35 m from interaction point [An92a, Pi93a].

After the luminosity upgrade, the old LUMI system can not be used anymore. This is mainly due to the increase in the amount of synchroton radiation and the increase in the critical energy of the synchroton radiation [Ze99a]. Therefore a major redesign of the old system was necessary.

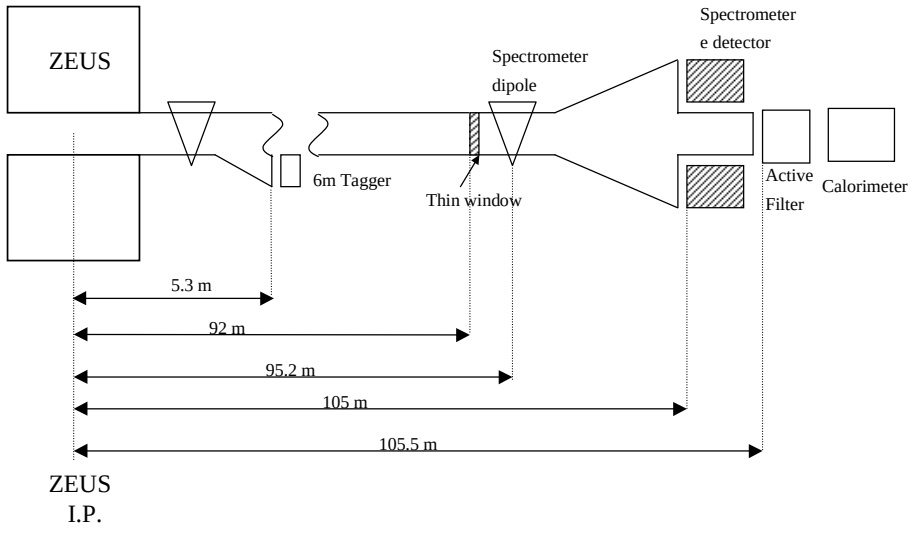

Figure 2.2: *The ZEUS lumi system [Ze99a].*

The new LUMI system consists of three detectors (figure 2.2):

- An upgraded version of the photon calorimeter: The Bremsstrahlung photons leave the beam pipe through an exit window 92 m from the interaction point. Then they pass through an active filter system and their energy is measured by a lead/scintillator sandwich calorimeter.
- The pair spectrometer: Part of the Bremsstrahlung photons which leave the beam pipe through the exit window undergo pair production in the window. The produced pair is then seperated by the magnetic field of

a dipole magnet. The e^- and e^+ are finally measured seperately by two tungsten/scintillator sandwich calorimeters (the former beam pipe calorimeter BPC).

- The 6m tagger. Electrons which radiated a Bremsstrahlung photon can leave the beam pipe through an exit window located 5.3 m from interaction point. There they are diverted by magnetic fields and hit a tungsten/ scintillator spaghetti calorimeter.

2.3 The 6m tagger

The general position of the 6m tagger can be seen in figure 2.1 and a more detailed view in figure 2.3. The available height can not be fully used, because above and below the tagger a cooling system will be placed.

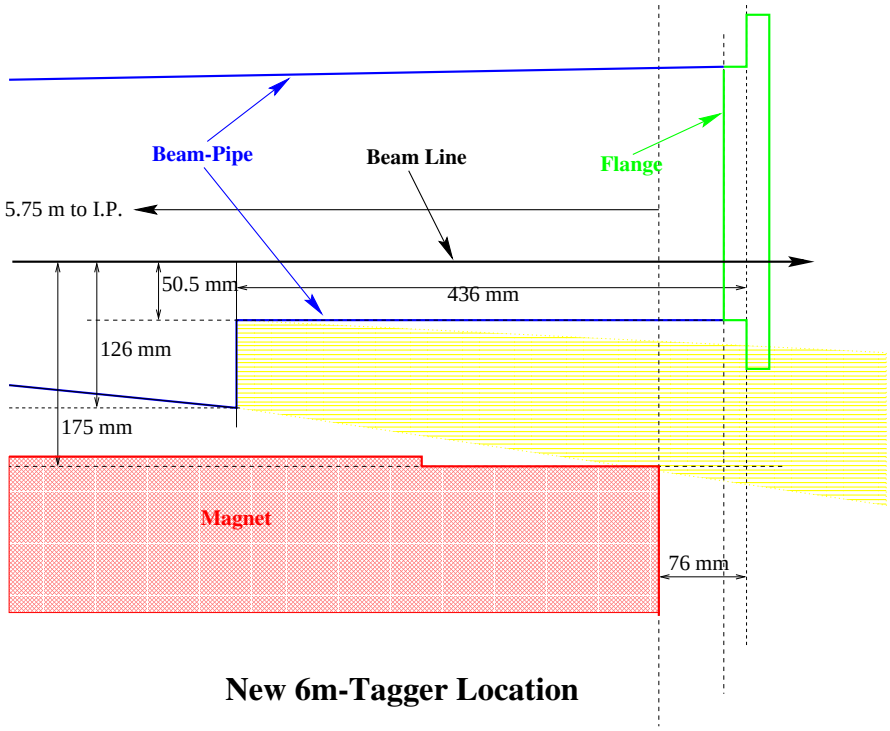

Figure 2.3: *Available space for the 6m tagger [Ze99a]. The maximum allowed height is* 30 mm. *The shaded area shows the paths of the electrons after leaving the beam pipe through the exit window.*

Due to the beam pipe geometry and the magnetic fields the 6m tagger has a near 100 % acceptance for electrons in the range of 5 GeV to 9 GeV (for positrons 4–8 GeV) [Ze99a] and can therefore be used to cross check the acceptance and the energy calibration of the photon calorimeter and the spectrometer. This is done by studying $e\gamma$ coincidences between 6m-tagger and the photon

calorimeter or the pair spectrometer using $E_\gamma + E_e = 27.5$ GeV. In addition to its use in the luminosity measurement, it can be used to study interactions at very small x.

Chapter 3

Detector description

3.1 Detector geometry

The 6m tagger will be installed in one of the HERA quadrupole magnets. This provides for a number of rather bad operating conditions:

- There is only limited space available (figure 2.3 on page 5).
- The tagger will be placed directly next to the beam pipe where it will be exposed to a high radiation background of aprox. 10–20 kGy / year. This requires choosing a radiation hard scintillator [La01a].
- The operating temperature of the magnet is about 50–70°C. This makes a cooling necessary because transmission of flourescense light decreases with time at elevated temperature [To01a]. This ageing effect is enlarged when the fibers are exposed to radiation [Zi03a].

The main design constraint for the 6m tagger is the limited space available. For a calorimeter to fit in there it must be constructed of a dense material with small radiation length and Molière radius. Only tungsten meets these criteria. To get a good energy resolution without reducing the density of the tungsten too much a spaghetti calorimeter design was chosen. Another advantage of the spaghetti calorimeter design is that it provides an easy way to transmit the light out of the magnet to the photomultiplier tubes (PMTs) by directly connecting the scintillating fibers to the PMTs [Ze99a].

For readout purposes the fibers are grouped into cells of 27 fibers. The fibers are SCSF-38M produced by Kuraray with a diameter of 0.5 ± 0.05 mm and 1.5 m in length. The geometry and grouping of these fibers can be seen in figure 3.1 and the notation of the 70 cells in figure 3.2. To be able to machine the detector, it hasn't been built out of a solid tungsten block, but out of tungsten plates. The exact geometry and production tolerances of these plates can be seen in figure 3.3.

The fibers of a single cell are all connected to and read out by a single PMT. For the PMTs the type R5600U from Hamamatsu has been used. The advantages of these PMTs are:

- Their compact size.

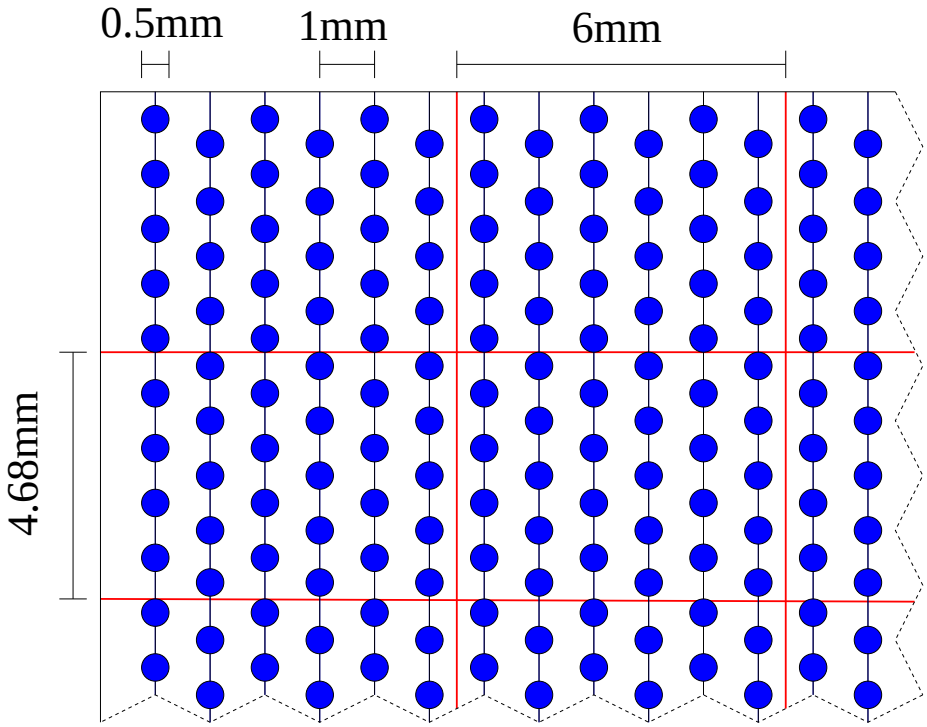

Figure 3.1: *Close up view of the edge of the detector from the front. The spacing and the size of the fibers and cells can be seen.*

50	51	52	53	54	55	56	57	58	59	5a	5b	5c	5d
40	41	42	43	44	45	46	47	48	49	4a	4b	4c	4d
30	31	32	33	34	35	36	37	38	39	3a	3b	3c	3d
20	21	22	23	24	25	26	27	28	29	2a	2b	2c	2d
10	11	12	13	14	15	16	17	18	19	1a	1b	1c	1d

Beam

Figure 3.2: *This is the way the cells are named in this thesis.*

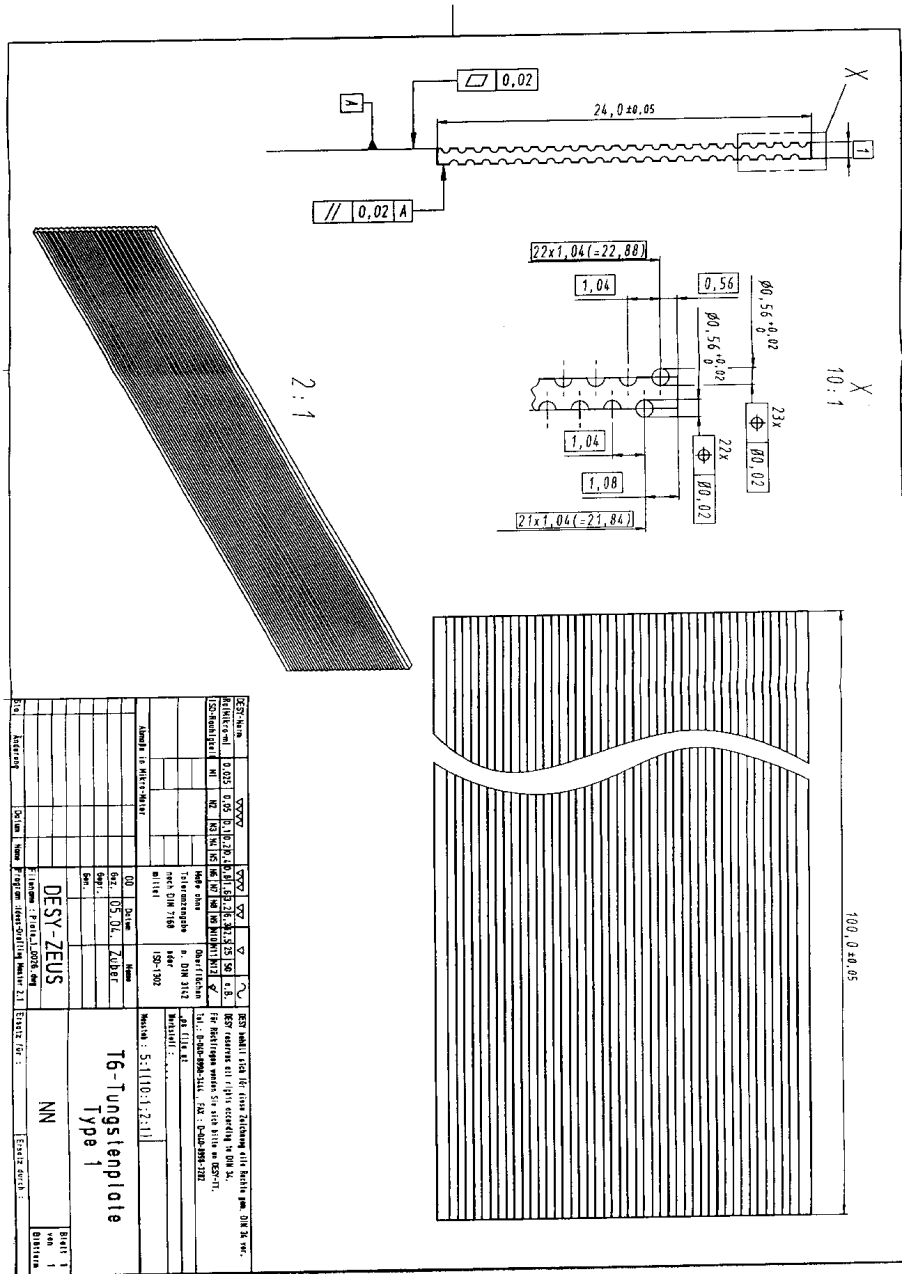

Figure 3.3: *Technical drawing of the tungsten plates used to assemble the detector.*

- Their insensitivity to magnetic fields.
- These PMTs were successfully used in the ZEUS forward plug calorimeter (FPC) [Ba99a] which was removed during the lumi upgrade shutdown to make space for the new beam pipe. Therefore these PMTs could be reused for the 6m tagger.

For testing purposes the PMTs are connected to LEDs by lightguiding fibers. The LEDs send short light pulses at a constant rate ($\sim$ 1 kHz). These light pulses can be used to monitor the stability of the PMTs.

Before the final detector was built, a half-sized prototype was built. For both the prototype and the complete detector testbeam measurements and simulation runs have been made. Prototype and detector differ in the following:

- The number of cells and thereby the size: The prototype had 6×5 cells (37×23 mm^2), while the complete detector has 14×5 cells (85×23 mm^2).
- The fibers of the final detector have been painted white at the end to increase the reflection coefficient and thereby the light yield and the longitudinal uniformity.
- The type of fiber used: The prototype used SCSF-81M because it has good radiation resistance. The detector used SCSF-38M because a study by [La01a] showed that these aren't damaged by prolonged exposure to light.
- The prototype contained a broken PMT connected to the cell 15.
- The prototype also used the PMT type R7400U from Hamamatsu have been used. The R7400U is an improved version of the R5600U that has a 30 % higher photo-electron yield. For the detector these weren't used as they turned out to be less linear.

3.2 Monte Carlo Simulation

To get an improved understanding of the detector a Monte Carlo simulation has been developed using the EGS4 code [Ne85a]. A first version has been given by Graciani [Gr00a]. A rewrite of nearly the complete code has been done for this thesis. At ZEUS the 6m tagger will be used to measure electrons with and energy of 4–9 GeV. The testbeam experiments have been made with energies of 1–6 GeV. This means that in the range from 6–9 GeV the simulation must be used to test the behaviour of the detector.

This simulation basically works by tracing the path of each particle or photon of the electromagnetic shower until it reaches a minimum energy of 10 keV or leaves the detector. The energy deposited in the fibers is taken as the signal of the PMT. Although other parameters are possible, only simulation runs with an angle of 5° with respect to hitting perpendicular and events distributed evenly over the front face of the detector have been used for this thesis.

The simulation also stores the energy deposited in the different regions of the simulated volume (i.e. fibers, absorber, above detector...) and the exact parameters of the incoming particle, which can be used for additional studies.

The output of the simulation is not the signals of the PMTs but the energy deposited for each fiber seperately divided lengthwise into 10 pieces of 1 cm length.[1] The program building the root trees takes the energy deposited in the different fiber segments and calculates from that the signal of the different cells.

The following information is contained in the simulation:

- the nominal geometry;
- the leckage losses at all 6 borders;
- the cell structure.

The following effects are not taken into account:

- differences in the primary light yield;
- differences in the PMT gain;
- quantisation effects by the ADCs;
- the attenuation length of the fibers;
- photostatistics of the PMTs;
- electronic noise within the readout;
- the broken PMT in the prototype;
- calibration uncertainties.

The simulation doesn't contain support for the following effects:

- beam quality, i.e. background events, energy resolution, uneven distribution of events over surface...;
- events hitting the side of the detector;
- the detector consists of individual tungsten plates; it is simulated as a tungsten block;
- production tolerances of the tungsten plates and the scintillator fibers;
- placement tolerances of the tungsten plates and the fibers, especially of the fibers that couldn't be inserted into the detector completely;
- the backshowering from the magnet at the upside and downside. But this isn't available at the testbeam either, therefore this only affects the final installation at ZEUS;
- different incident angle;
- external magnetic fields which were not present at the testbeam but are in ZEUS since the tagger is installed inside a magnet.

For ZEUS, a Monte Carlo simulation is also needed which can be integrated into the ZEUS Monte Carlo MOZART [Wi01a] and which accounts for the important effects not reproduced by the simulation used for this thesis.

[1] Actually I'n not sure wether there might be a bug in the simulation that causes the energy to be deposited at the wrong position within the same fiber. This effect would only happen, if the particle moves along a fiber and crosses the border between two fiber segments, but would probably make studies changing the longitudinal uniformity of the fibers less usefull.

3.3 The EGS4 package

In this section a *short* description of the EGS4 code package [Ne85a] is given.

EGS4 basically provides for the ability to simulate electromagnetic showers. To do that it follows the path of one particle at a time calculating the energy it loses by moving through matter and letting it create new particles on a random basis. The particles are dropped on user request or if they reach a minimum energy. EGS4 allows the user to store data about the movement path of the particles and about the energy they deposit.

The user is responsible for creating the initial particles, defining the geometry and storing the data needed. To be able to differentiate between the different media the simulated object is divided into regions each with its own medium.

To create a new particle, the simulation has to call the function `SHOWER` with the correct parameters. Usually all results are stored in some global variables that will be saved and reset between the calls.

To be able to store the data needed the user sets up an event handler called `AUSGAB` which selects the events of interest. The event handler gets all available data about the particle (like energy, position...) which can then be used to obtain the desired information.

To define the geometry another user supplied event handler, `HOWFAR`, is used, that is called everytime a particle might move. It is supplied with the current region, the position, the movement direction and the movement distance. If the particle would leave the current region, the event handler has to reduce the movement distance and set the new region accordingly. If the particle should not be followed anymore, the event handler has the option to drop it.

In moving the particle EGS4 simulates the following reactions:

- Bremsstrahlung production;
- electron-positron annihilation;
- Molière multiple scattering;
- Møller and Bhabha scattering;
- continuous energy loss applied to charged particle tracks between discrete interactions;
- pair production;
- Compton scattering;
- photoelectric effect.

Not included are:

- the production of flourescent photons and Auger electrons;
- coherent (Rayleigh) scattering (also available as option)

Chapter 4

Reconstruction Algorithms

In this chapter, the various reconstruction algorithms used to calculate the energy or position of the incoming particle are described. A reconstruction is an algorithm calculating one or more kinematic variables from the signals of the different channels. The different algorithms can be divided into two types:

- global reconstructions which compute their result using all cells of the detector and treating all of them equally;
- local reconstructions which compute their result using only the cells in a region around a "central cell" and which not necessarily treat all cells equally.

Global reconstructions have the advantage of not requiring the definition of a central cell but have the disadvantage of dealing mainly with cells containing only noise. For local reconstructions, most cells have a high signal to noise (S/N) ratio but it requires the definition of a central cell.

4.1 Reconstruction regions

The incoming electron produces an electromagnetic shower, hence its energy is distributed over several cells. As the detector is rather large compared to the shower size, most cells contain no signal and can therefore be omitted in the reconstruction. To do this, the reconstruction is using only a subset of all cells called reconstruction region. To define this reconstruction region, a central cell is defined which marks the center of the reconstruction region. The central cell is chosen to be the cell with the highest signal.

Around the central cell three reconstruction regions are defined:

- A region of 5 times 5 cells around the central cell. If the central cell is too close to the border the region is moved so that it will fit completely onto the detector. As a canonical choice of the fiducial volume one can select all the cases in which the region doesn't have to be moved (figure 4.1). The simulation shows that 97 % of the signal is contained in these cells (for the fiducial volume).

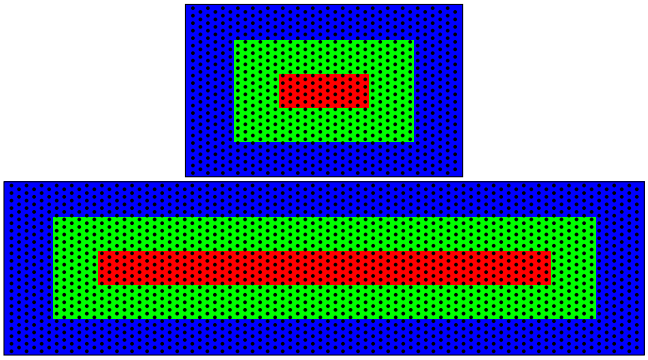

Figure 4.1: *Front view showing the fiducial volumes for prototype (top) and detector (bottom). The central region is the region available for the* 5×5 *reconstruction region. For* 3×3 *cells everything except the border can be used.*

- A region of 3 times 3 cells can be build in the same way. The simulation shoes that 89 % of the signal is contained in these cells (for the fiducial volume).

- As another possibility, global reconstructions use all cells. Although this region contains all of the signal, the simulation shows that it only contains 90 % of the energy and the rest is lost due to leakage (for the 5×5 fiducial volume).

Really used are only the 3×3 and 5×5 regions. The 5×5 region gives a slightly better resolution, because it contains nearly the complete shower. The 3×3 region gives a much bigger fiducial volume, because it is much smaller. Global reconstructions are not used, because they have a slightly smaller fiducal volume than 5×5 and a worse resolution than 3×3 cells.

4.2 Energy reconstruction

The most important variable the tagger has to determine is the energy of the incoming particle. The calibration was chosen in a way that each cell gives the same signal for a given energy deposit. For every reconstruction region, the energy can be reconstructed by summing up the signals in all cells in the region. In labelling the axis of a plot these are often called e5, e3 and eAll.

The energy resolution of a calorimeter can be examined by plotting the relative resolution (i.e. the energy resolution divided by the energy) against the energy. This plot is fitted with one or more of the following terms. If more than one term is fitted they are added in quadrature:

- Noise $\Delta E_{noise}/E \propto 1/E$: These are energy independent effects like electronic noise.

- Statistic $\Delta E_{stat}/E \propto 1/\sqrt{E}$: These are mainly statistical effects which are energy dependent in that the number of random decisions is proportional to the energy like for sampling fluctuations and photostatistics.

- Leakage $\Delta E_{leak}/E \propto \ln E$: This term is mainly caused by longitudinal leakage of an electromagnetic shower.
- Constant $\Delta E_{const}/E \propto 1$: This term is caused by effects proportional to the energy which are mainly non-linearities and non-uniformities, e.g. a bad calibration of a single channel will cause such a decrease in resolution.

4.3 Position reconstruction

4.3.1 Basic reconstruction

The other variable reconstructed is the position of the incoming particle. To determine the position the center of the shower, i.e. the center of the deposited energy, is determined. For example, the x-position can be reconstructed using energy weighed sums:

$$\bar{x} = \sum_i x_i \cdot S_i \Big/ \sum_i S_i \tag{4.1}$$

where x_i is the position of the cell i and S_i the signal of cell i. The sums are done over all cells in the reconstruction region except the cells that are in rows that have a negative energy sum (this can only happen in low energy events where the noise is bigger than the signal). In the same way, the y-pos. is reconstructed.

This reconstruction can be done for all reconstruction regions, but it makes little difference which of the three reconstruction regions is chosen. Because it has the largest fiducial volume only the 3×3 reconstruction was studied. In plots it is often called xL3.

This reconstruction has several disadvantages, mainly its non-linearity (figure 4.2):

- Because the shower is not fully contained in the reconstruction region, the part of the shower used is not completely symmetrical, resulting in a shift of the reconstructed position, causing a slight non-linearity. This effect can be studied in the simulation and compensated quite well.
- If the shower is not contained in the calorimeter, the shower will change shape as leakage losses increase, causing another non-linearity in the reconstruction. This effect can be studied in the simulation and compensated quite well.
- The shower maximum is shifted with respect to the impact position on the detector front. This shift depends on the incident angle and energy, resulting in a non-uniformity. This effect can also be studied and compensated by using the simulation. Because at ZEUS the angle and energy of the Bremsstrahlungselectrons are position dependent this may also introduce another non-linearity.

4.3.2 Corrected reconstruction

To improve the position reconstruction and compensate for the first two non-linearities listed above, results from the Monte Carlo simulation have been used.

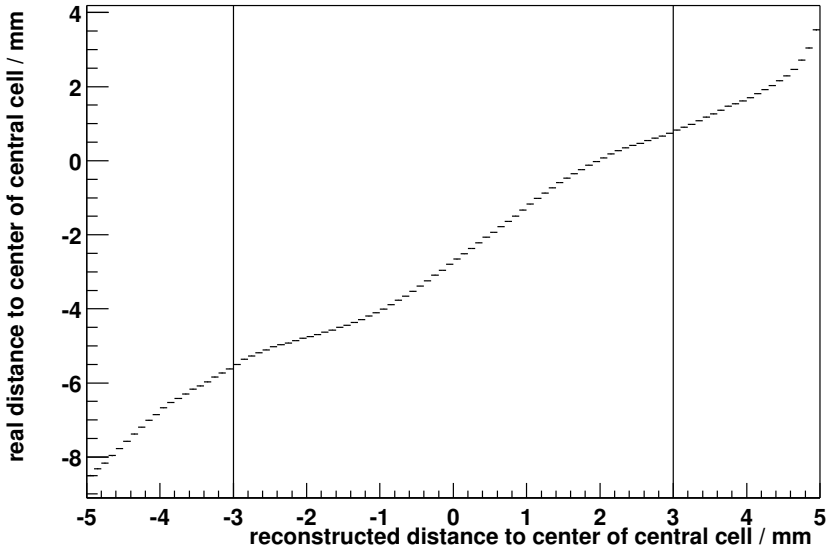

Figure 4.2: *Simulation of the correlation between reconstructed position of the shower maximum using the basic reconstruction and the real incident position at the front face of the detector. The offset is caused by the particles hitting non-perpendicular. The vertical lines mark the borders of the central cell. This plot was generated using simulation data at* 4 GeV *and a* 3×3 *reconstruction region.*

For the simulation the incident position of the particle on the front face of the detector is exactly known. The correspondence between this position and the reconstructed position can be used to correct the reconstructed position. For this correction not the absolute position, but the distance to the center of the reconstruction region is used.

The reconstructed distance is used to seperate the data in 0.1 mm wide stripes. For each of these stripes, the distribution of the distance of the known incident position from the center has been plotted and fitted with a Gaussian curve. The mean values of these fits have been plotted against the reconstructed distance (figure 4.2). The result was parameterized by a polynominal. The corresponding parameters (except for the constant term) are used to correct the basic reconstruction. The constant term hasn't been used, because it's dependent on the energy and angle of the incident particle. In plots this reconstruction is often called xL3c.

This correction can be applied to experimental and simulation data without the need to know the exact incident position. But these correction factors has only been calculated for 4 GeV electrons which hit the prototype under an angle of 5°. If this reconstruction is to be used at ZEUS it should be checked wether it works correctly at all energies and angles, and also if it can be improved by including electronic noise in the simulation.

Chapter 5

Measurements with the prototype detector

5.1 Testbeam setup

The prototype of the 6m tagger has been tested at the DESY testbeam facility in August 2000. The testbeam setup is shown in figure 5.1. The electrons were hitting the prototype under an angle of 5°. They were triggered by using two crossed finger counters T2H and T2V with exchangable fingers of 2, 5 and 20 mm width. The trigger was placed in the center of the beam to get the maximum rate. To change the position of the beam the detector was moved. The high voltage was adjusted so that all channels showed the same signal if pulsed with the LED.

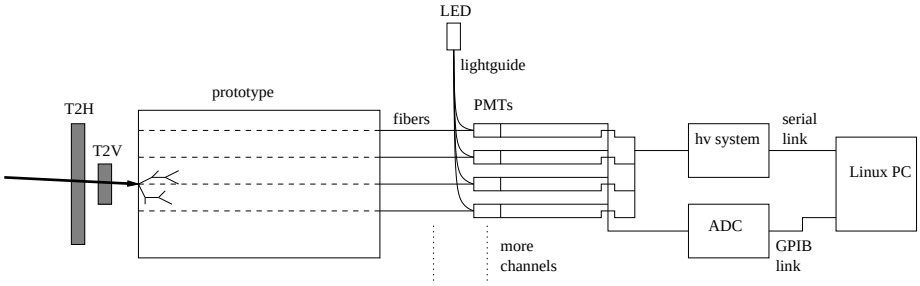

Figure 5.1: *Schematic drawing of the setup used during the 1st testbeam.*

Because no veto counter and no trigger directly in front of the collimator was used the measurements suffered from a rather large background which had to be compensated for. This was achieved by applying a cut on the width of the shower to be smaller than 8 mm. The width is connected to the size of the shower and thereby should be bigger for electrons which have showered before hitting the tagger. The size of 8 mm was chosen because it is bigger than the shower sizes observed in the simulation and also bigger than the shower sizes observed for events with the expected energy (figure 5.2), but smaller than the width expected from an electron that showered already before hitting the tagger.

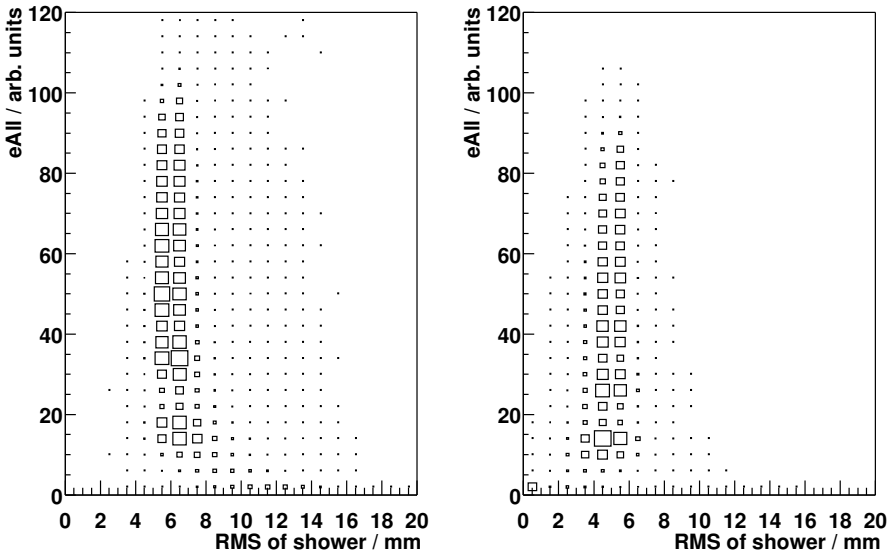

Figure 5.2: *Shower width at energies 1–6* GeV *for testbeam measurement (left) and simulation (right). On the y-axis the energy sum eAll over cells is plotted. To eleminate background events, a cut for a shower width smaller than* 8 mm *is applied for the analysis.*

This cut was always applied except for those cases in which it will be stated otherwise.

5.2 Calibration

In order to calibrate the detector 4 GeV electrons were used. To ensure all cells were hit evenly each cell was measured using a 5×5 mm^2 trigger in front of it. The goal of calibration for this testbeam was to get the same signal response as for the simulation.

The calibration was done in two steps. In the first step, each event is used in the calibration of the cell which has the highest signal in that event (without a cut on the shower size). In the second step, the signals in the neighbouring cells have been used to select events which seem to hit in the center of the cell. The resulting calibration constants can be seen in table A.1. The calibration constant is defined as a constant divided by the measured signal. The calibration constants of the second step have been applied to the data before the other studies were done.

In the first step the signals of all channels were highly different. Therefore as little comparison between the channels has been done as possible. Therefore I decided to use for each event only the information of the cell with the maximum signal.[1] The resulting spectra (figure A.1 on page 45) are assumed to have

[1] An alternative here would be to use the known trigger position to select the cell. This showed little difference and therefore wasn't used here. An additional reason is that this

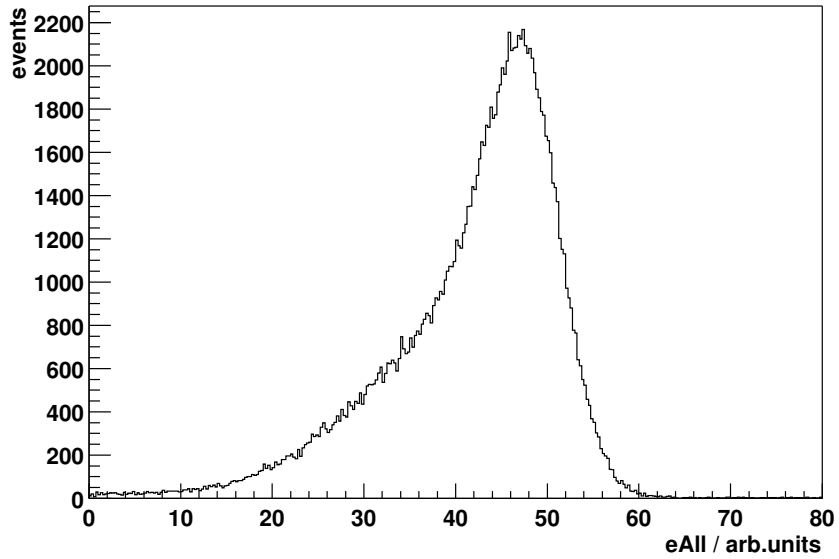

Figure 5.3: *Energy sum eAll over all cells for the calibration events after applying a cut on the shower size. For the second calibration step, only the events with energies between 40 and 75 where used.*

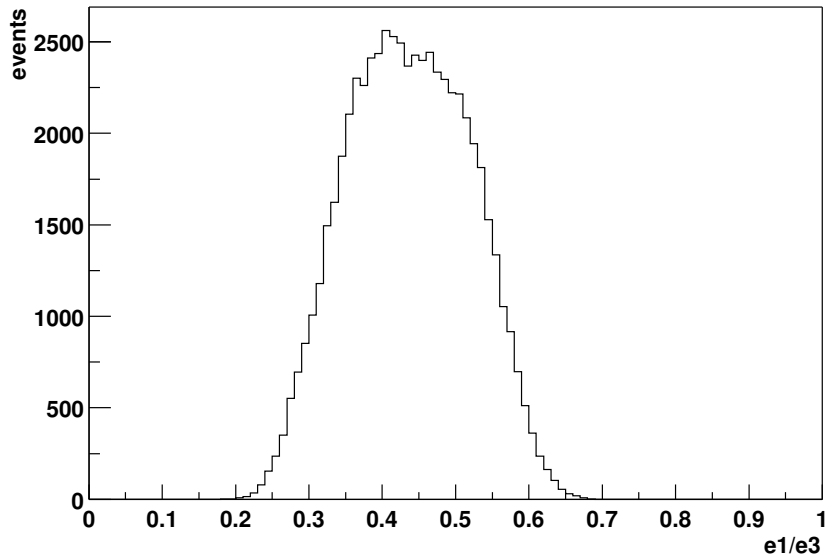

Figure 5.4: *Ratio of the signal e1 in the central cell to the sum e3 of the signals in the* 3×3 *reconstruction region. For the calibration only events with a ratio greater than* 0.6 *have been used. For this plot, all other cuts used for calibration and a cut for* 3×3 *fiducial volume have been applied.*

a Gaussian shape, corresponding to a hit in the center of the cell, and a low energy tail, caused by background and non-central events. Therefore a Gaussian curve was fitted starting at the mean value of the distribution. The calibration constants were then adjusted so that the mean values of all fits were the same. Because this calibration method uses only the part of the spectrum with the highest signal, it was named max channel endpoint calibration.

In the second calibration step, a number of additional cuts have been applied. The main goal being to make a sharp definition of the incident position causing the signal to become Gaussian. The first cut used is the usual cut on the shower size to get rid of background events (section 5.1). The next cut is used to select the events where the total energy is in the expected range (figure 5.3). For high energies this is mainly done to avoid problems in the read out (from time to time the readout generated events with a much to high energy). For low energies this is done to eliminate events which are to close to the detector border. An additional cut is used to select for central events where the central cell contains at least 60% of the energy of the 3×3 energy reconstruction (figure 5.4). Figure A.2 on page 46 shows that the resulting spectra have nearly Gaussian shape.

Both calibration steps have also been done with simulation data. This was done for two reasons. The first was to calibrate the testbeam data so that it showed the same signal heights as for the simulation. More importantly, this calibration has been used to get a compensation factor for the leakage losses in the border cells. Unfortunately this wasn't possible for the left border, because no simulation data was available which got close enough to the left border. Therefore I chose to correct the left border with the same factor obtained for the right border. For the left and right column the correction factor is 1.073 and for the top and bottom row it is 1.015. For the corners the geometric mean of both was used.

A different approach was taken in [La01a] by using the corrected position reconstruction to select only events in the center of the cell. This approach has several disadvantages:

- it is contaminated with background events at low energies;
- at the border the position reconstruction isn't as exact as needed causing the low energy tail to remain;
- because of the low energy events, the fits must still be done with a lower limit;
- It doesn't correct for the border cells showing a different response to the same calibration.

5.3 Energy scan

To test the linearity and the resolution of the energy reconstruction, measurements at the energies 1, 2, 3, 4, 5 and 6 GeV have been performed. For each energy two measurements with a 20×20 mm^2 trigger have been done: one on

information isn't available at the final installation at ZEUS, but this method can still be applied there using kinematic peak events.

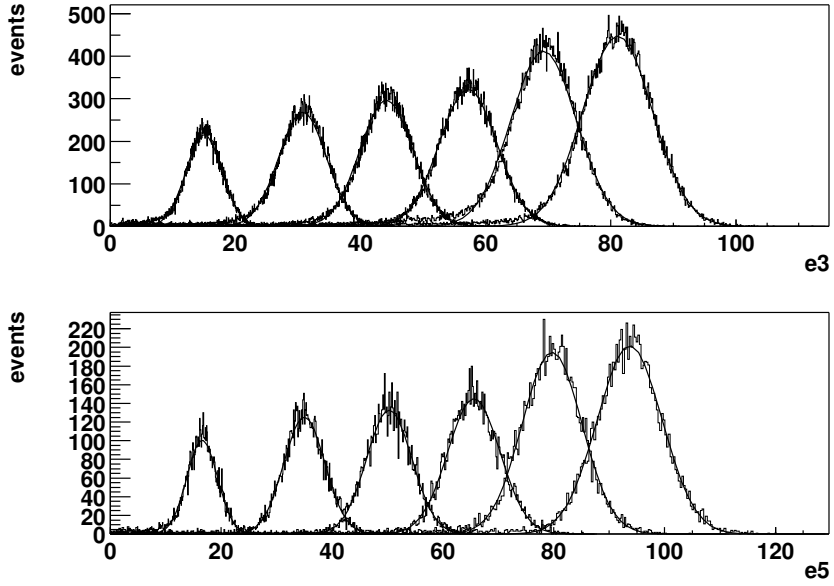

Figure 5.5: *Energy spectra for the testbeam data with 1, 2, 3, 4, 5,* 6 GeV *beam energy. Cuts for fiducial volume and background (see section 5.1) have been applied. The rise in the number of events is probably caused by increasing beam quality.*

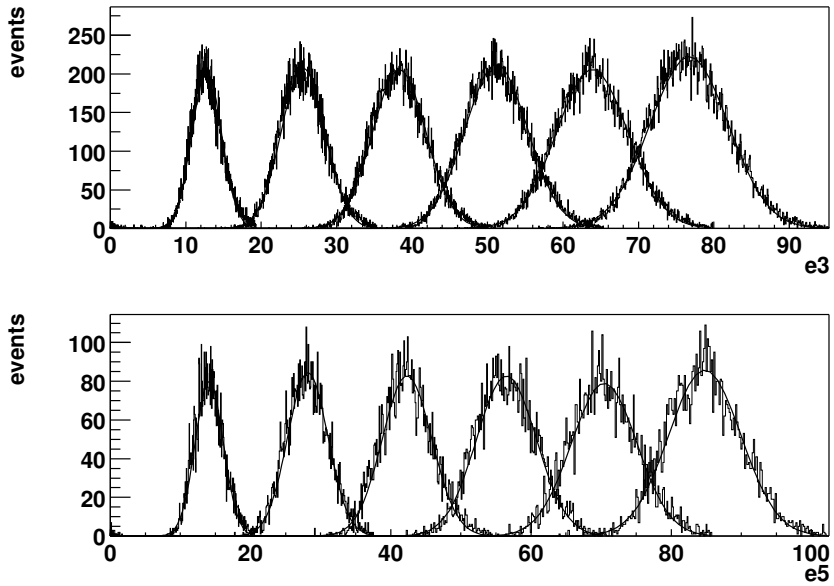

Figure 5.6: *Energy spectra for the simulated data. Same plot as in figure 5.5.*

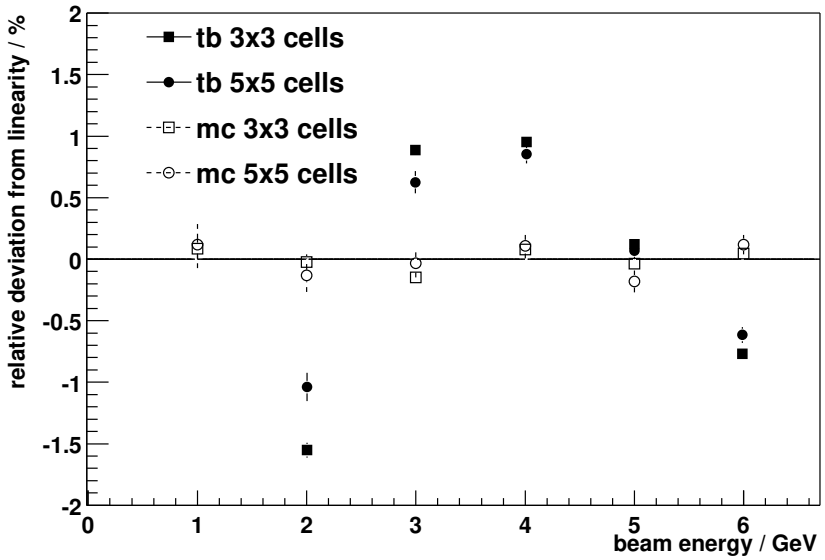

Figure 5.7: *Deviation from linearity for testbeam (tb) and simulation (mc) data. This plot has been generated by plotting the reconstructed energy over the beam energy, fitting with a straight line and calculating the relative differences. For* 1 GeV *the testbeam data is very unprecise and therefore not included in the plot.*

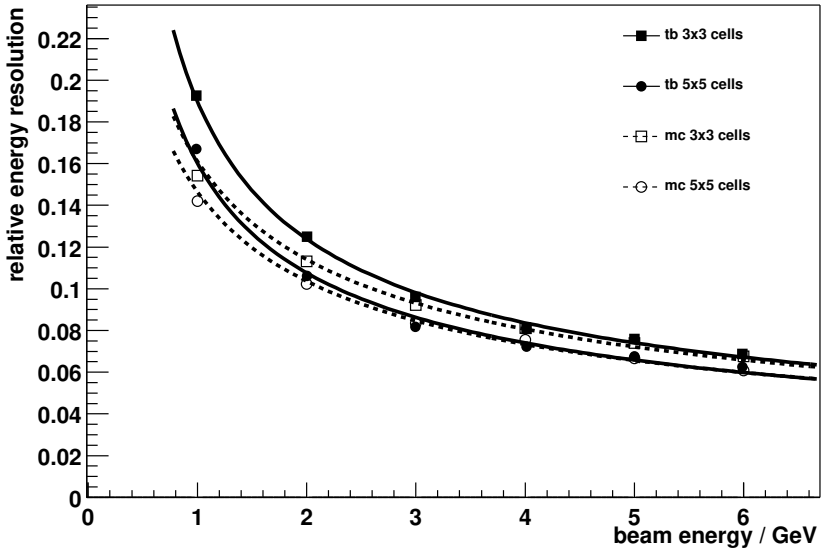

Figure 5.8: *Energy resolution of the prototype determined from testbeam (tb) and simulation (mc) data. For each energy the ratio of sigma to mean of the energy spectrum is plotted. The curves correspond to the fit results using equation 5.1.*

the left and one on the right side of the prototype. The resulting spectra can be seen in figure 5.5 and in figure 5.6

With these measurements, the energy sums in 3×3 and in 5×5 cells have been calculated. For each energy the energy spectrum has been plotted and fitted with a Gaussian curve.

To determine the linearity the mean of the fits was plotted against the energy and fitted with a straight line. The relative difference of data and fit has been plotted against the energy (figure 5.7). For the testbeam data in the energy range of 2–6 GeV the deviations from linearity are less than 1.5 %. The results of the simulation are perfectly linear.

To determine the energy resolution the ratio of sigma ΔE to mean E (of the fit values) was plotted against the energy and the function

$$\frac{\Delta E}{E} = \sqrt{\left(\frac{\Delta E_{noise}}{E}\right)^2 \cdot \frac{1}{E_B^2} + \left(\frac{\Delta E_{stat}}{E}\right)^2 \cdot \frac{1}{E_B}} \tag{5.1}$$

was fitted (figure 5.8) where $\Delta E_{noise}/E$ and $\Delta E_{stat}/E$ are the parameters of the fit and E_B is the beam energy. This results in the resolutions given in table 5.1. As can be seen the simulation has a noise term of 0 which is expected, as the simulation doesn't contain noise simulation. The statistical term is nearly the same for experiment and simulation, which shows that the simulation is working well for the energy resolution. This means that the photostatistics has no influence on the resolution of the prototype.

data	reconstruction region	$\Delta E_{noise}/E$	$\Delta E_{stat}/E$
tb	5×5	7.1%	14.4%
tb	3×3	10.4%	15.9%
mc	5×5	0.0%	14.7%
mc	3×3	0.0%	16.1%

Table 5.1: *Results of the fits for the energy resolution of the prototype (figure 5.8) both for testbeam (tb) and simulation (mc).*

5.4 Fine scan

Three horizontal scans have been performed on the prototype each over one of the inner rows. Each of these scans has been done at 4 GeV using a 2×5 mm^2 trigger moving in steps of 2 mm. These scans can be used to study the uniformity of the energy reconstruction and to test the linearity and resolution of the position reconstruction.

To test the uniformity of the energy measurement, the deposited energy is plotted for each trigger position without using a cut on the fiducial volume. To this distribution a Gaussian fit is made. The mean values of these fits are plotted against the trigger position (left side of figure 5.9).

A more detailed look at the uniformity can be obtained by studying the relative difference between the energy and the mean of all energies (right side of figure 5.9). For the 3×3 reconstruction this has been done over all positions

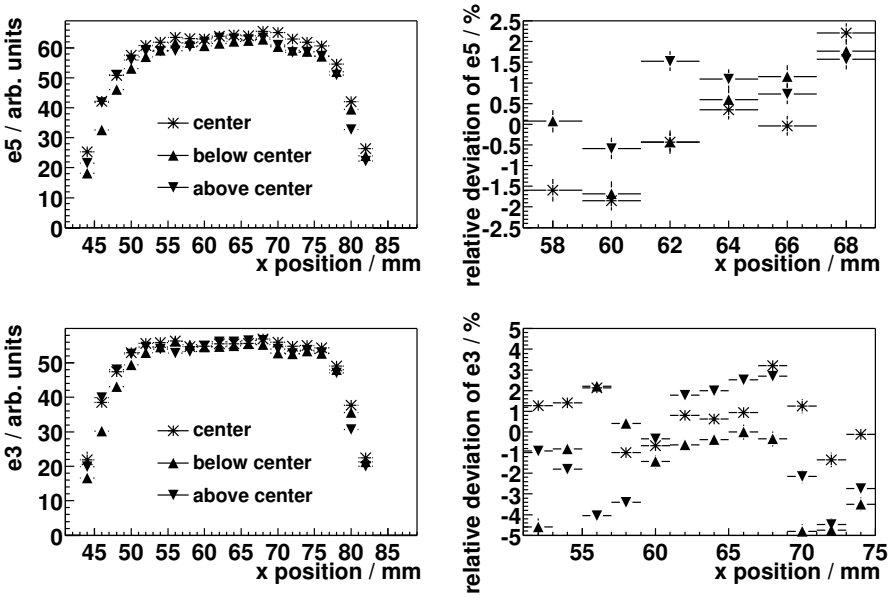

Figure 5.9: *Energy uniformity of the prototype for the testbeam data for* 5×5 *cells (e5) and* 3×3 *cells (e3). On the left the reconstructed energy is plotted against the position, on the right the relative deviation from the mean is shown.*

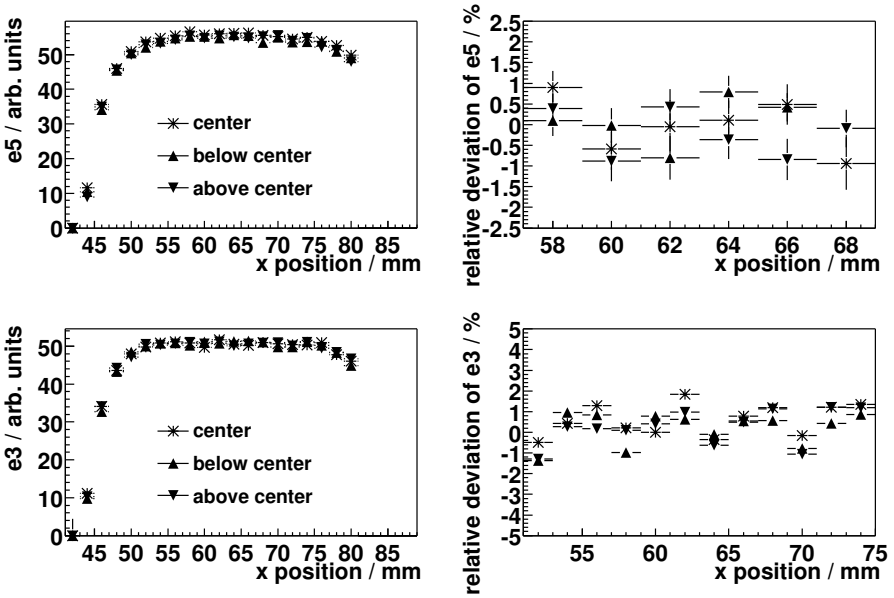

Figure 5.10: *Energy uniformity of the prototype for the simulated data. The plot is the same as in figure 5.9.*

inside the fiducial volume. For the 5×5 reconstruction only the central row hits the fiducial volume, therefore this test has been done seperately for every row using the cells which hit the fiducial volume in x direction.

Figure 5.9 shows that the 3×3 reconstruction has non-uniformities which are smaller than 5%. The 5×5 reconstruction shows a higher signal in the center than near the border, but shows non-uniformities within each row which are smaller than 2.5%. This isn't too surprising, as the 5×5 reconstruction averages over 5×5 cells, reducing the effects of a single miscalibrated cell. Another reason is, that for 5×5 cells we have only looked at the uniformity for 6 positions, which might be too small to see the real extend of the non-uniformity.

In figure 5.10, the same study has been done for the simulation. It shows non-uniformities which are within 2% for 3×3 cells and within 1% for 5×5 cells. This is significantly smaller than for the testbeam data showing that probably most of the non-uniformity of the testbeam data is caused by bad calibration and differences in light yield between individual fibers. Another interesting effect in the simulation data is that most of the non-uniformity for 3×3 cells is caused by a drop in energy every 6 mm. This is caused by the beam hitting between two cells and thereby being most near to the edge of the reconstruction region. Near the edge the signal is a little smaller because more signal is deposited outside of the reconstruction region, but this effect is to small to be seen for the testbeam data.

To test the linearity of the position reconstruction for every trigger position the reconstructed x position is plotted and fitted with a Gaussian curve. The mean values of these fits are plotted against the trigger position. To further test the linearity for each row a line with slope -1 has been fitted to the results and the difference between the values and the fit has been plotted.

This has been done for the basic and the corrected position reconstruction (see section 4.3). Figure 5.11 shows that the basic reconstruction is linear within 0.8 mm, whereas the corrected position reconstruction is linear within 0.4 mm. Comparing this with the simulated data (figure 5.12) with a linearity of 0.8 mm and 0.2 mm respectively shows that the non-linearities of the basic reconstruction are dominated by the non-linearities of the reconstruction algorithm whereas the non-linearities of the corrected reconstruction must have other causes.

To test the position resolution, the sigma of the gauss fit was plotted against the x position (figure 5.13). A sigma of 1.3 mm for the testbeam and 0.79 mm for the simulation was obtained. This resolution contains also the trigger width (2 mm). After correcting for the trigger width, a resolution of 1.1 mm and 0.42 mm, respectively, was obtained. This shows that the resolution of the position reconstruction isn't reproduced accurately by the simulation. One possibility would be that the electronic noise or the photostatistics decrease the resolution.

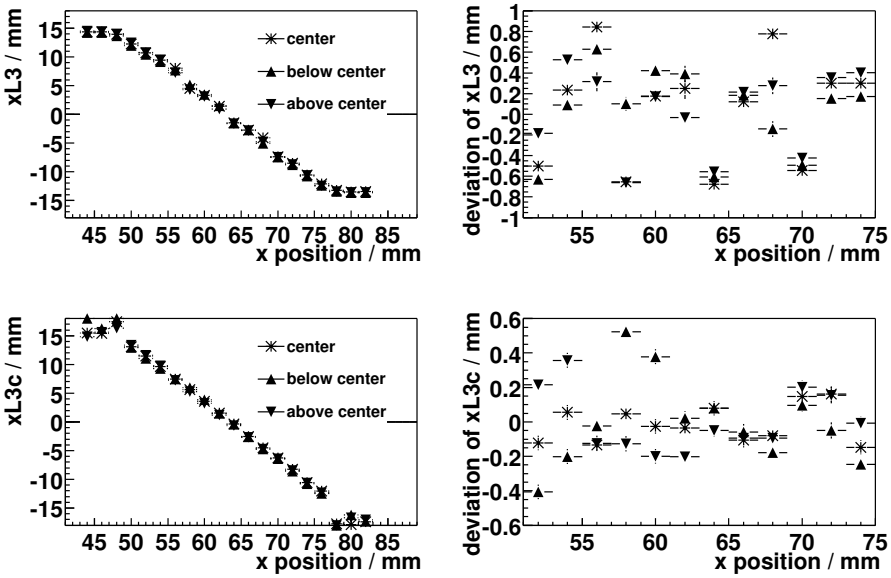

Figure 5.11: *Linearity of the basic (xL3) and corrected (xL3c) position reconstruction for the testbeam data. On the left side the reconstructed position is plotted against the real position, on the right side the deviation from a fit with a straight line is plotted.*

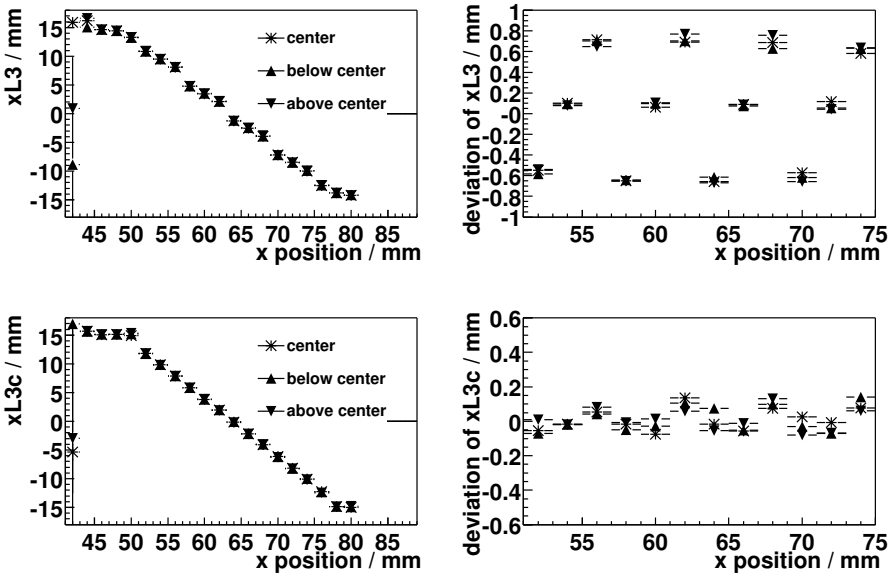

Figure 5.12: *Linearity of the position reconstruction for the simulation data. Same plot as in figure 5.11*

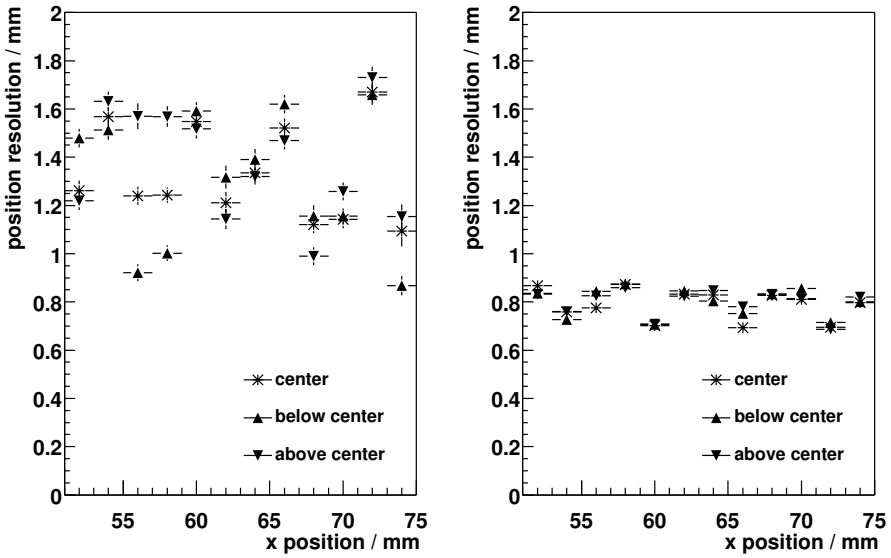

Figure 5.13: *Position resolution using a* 2 mm *trigger. The width of the distribution of reconstructed positions is plotted against the position. On the left for testbeam data, on the right for simulation data.*

5.5 Summary of testbeam measurement

The prototype has been successfully calibrated with the newly devised calibration method.

The energy reconstruction is linear within 1 % and has a resolution of

$$14.4\%/\sqrt{E} \oplus 7.1\%/E \quad \text{for } 5 \times 5 \text{ cells} \tag{5.2}$$

$$15.9\%/\sqrt{E} \oplus 10.4\%/E \quad \text{for } 3 \times 3 \text{ cells} \tag{5.3}$$

where E is given in GeV. Within the fiducial volume the energy reconstruction was shown to be uniform within 2.5 %, and 5% respectively, which is a factor 2.5 larger than for the simulation.

The position reconstruction was shown to be linear within 0.4 mm and to have a resolution of 1.1 mm. These values could not be reproduced by the simulation.

Chapter 6

Measurements with the complete detector

6.1 Testbeam setup

The complete 6m tagger has been tested at the DESY testbeam facility in april 2001. The testbeam setup is shown in figure 6.1. The electrons were incident on the detector under an angle of 6°. They were triggered using the trigger T3 directly in front of the beam pipe exit window and in coincidence with at least one of the following counters:

- the paddle S3;
- the finger counters T1 or T2;
- a minimum signal in the tagger (at least 10 pC).

To further constrain the beam a veto counter with a 3 mm hole (S1) was used during some measurements. The triggers (except T3) were placed in the center of the beam directly in front of the tagger. To change the position of the beam the detector was moved using calibrated stepping motors. If not otherwise noted the coordinates of the motors are used as the position of the beam on the tagger.

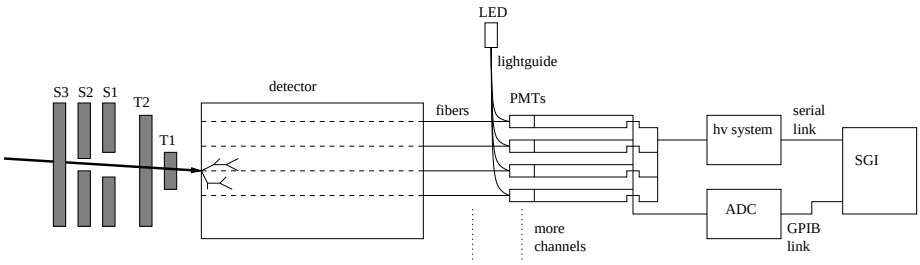

Figure 6.1: *Schematic drawing of the setup used during the 2nd testbeam measurement. Additionally another trigger (T3) has been placed directly in front of the beam pipe window.*

6.2 Calibration

During the first testbeam every cell was targetted individually using a trigger placed in front of it. But the calibration method doesn't need this position information, therefore the calibration data for this testbeam was taken using events distributed over the complete detector.

Because this method is rather fast, the high voltage was adjusted two times during the testbeam using the first step of the calibration method described in section 5.2. The goal of these calibrations was to get about 8 pC / GeV.

After the testbeam the complete calibration described in section 5.2 was done for the data taken with the last high voltage setting. The most notable differences to the calibration of the first testbeam are the electron energy of 5 GeV and the missing cuts on the shower size. Because this time the measured signal had a direct physical meaning (the signal in pC) the goal of the calibration was that the mean of the calibration constants remains one (although it is just 97 %). The resulting spectra of the first step can be seen in the figures A.3 and A.4. The resulting spectra of the second step can be seen in the figures A.5 and A.6.

6.3 Energy scan

To test the energy reconstruction measurements at energies of 1, 2, 3, 4, 5 and 6 GeV have been performed. Additionally simulation runs with up to 27 GeV have been done to study the detector response at high energies. Events distributed evenly over the detector were used and then cuts on the fiducial volume were applied to obtain the energy spectrum. Each of the resulting spectra was fitted with a Gaussian curve and the mean and sigma parameters of that fit were used to study the energy reconstruction.

To determine the deviations from linearity, the mean of the fit was plotted against the energy. This plot was fitted with a line and the relative difference between the data and the fit was calculated (figure 6.2). Deviations from linearity of less than 0.8 % for 3×3 and less than 1.3 % for 5×5 cells were observed. For the simulation runs the non-linearities are smaller than 1% (figure 6.3), but for the much harder condition to be linear up to 27 GeV.

To determine the resolution of the energy reconstruction, the relative energy resolution $\Delta E/E$ is plotted against the beam energy (figure 6.4). This gives an energy resolution of

$$17.0\%/\sqrt{E} \oplus 15.7\%/E \quad \text{for } 5 \times 5 \text{ cells} \tag{6.1}$$

$$18.4\%/\sqrt{E} \oplus 12.4\%/E \quad \text{for } 3 \times 3 \text{ cells} \tag{6.2}$$

where E is given in GeV. These values are slightly higher than the ones observed for the prototype and the angle and gate length study later on. This is partly due to the fact that this data was taken over more than one week and partly due to the fact that most of the other data was just taken at one fixed position.

For the simulation runs more resolution terms could be fitted resulting in the resolutions:

$$14.1\%/\sqrt{E} \oplus 0.0\%/E \oplus 1.2\% \oplus 0.0\% \cdot \ln E \quad \text{for } 5 \times 5 \text{ cells} \tag{6.3}$$

$$15.8\%/\sqrt{E} \oplus 0.0\%/E \oplus 1.3\% \oplus 0.0\% \cdot \ln E \quad \text{for } 3 \times 3 \text{ cells} \tag{6.4}$$

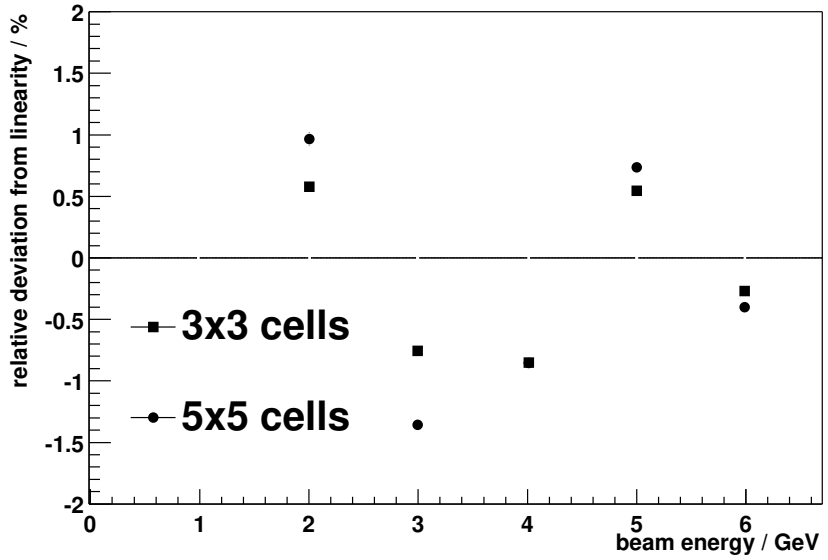

Figure 6.2: *Deviation from linearity for testbeam data. This plot has been generated by plotting the reconstructed energy over the beam energy, fitting with a straight line and calculating the relative differences. For* 1 GeV *the data are not included in the plot, because the fit to the energy spectrum was problematic.*

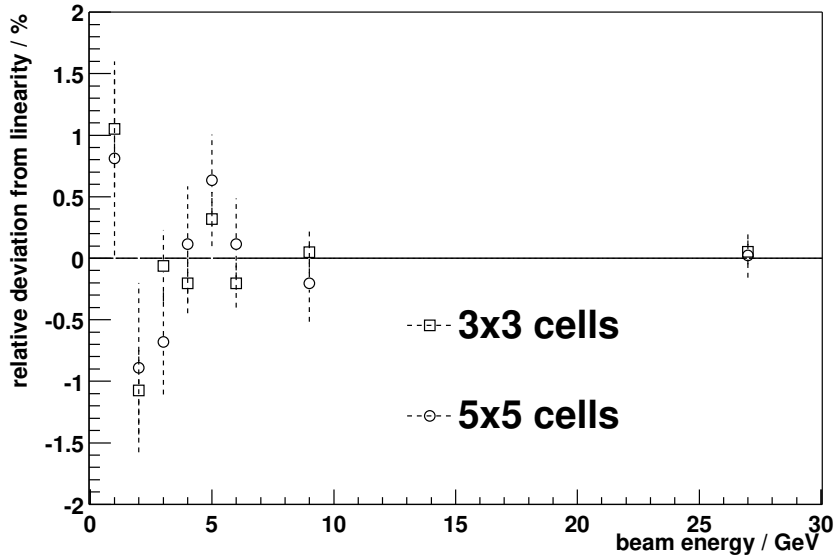

Figure 6.3: *Deviation from linearity for simulation data. This is the same plot as figure 6.2 but it goes up to* 27 GeV.

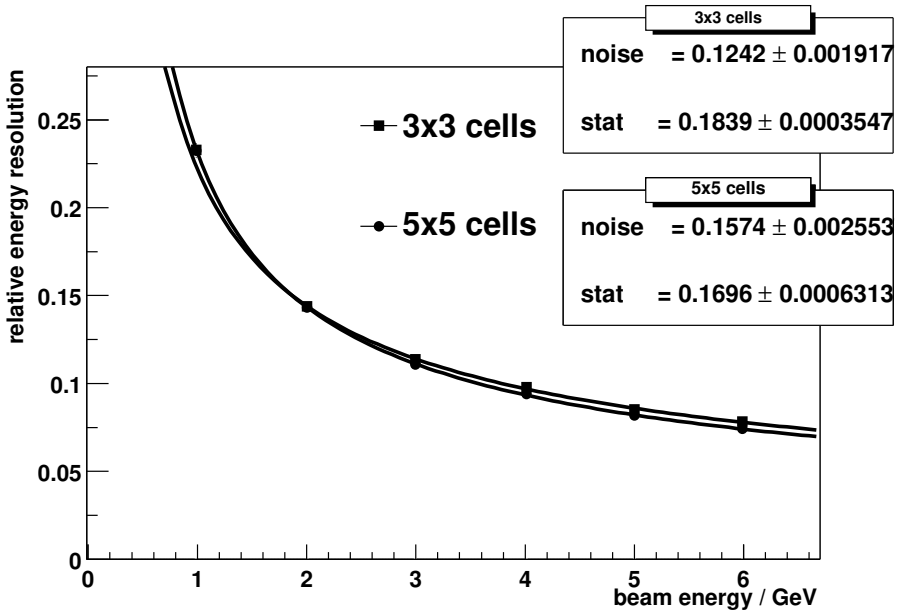

Figure 6.4: *Energy resolution of the detector for testbeam data. For each energy the ratio of sigma to mean of the energy spectrum is plotted. The curves correspond to the fit results using equation 5.1. The* 1 GeV *point was omitted from the fit, because it wasn't very precise.*

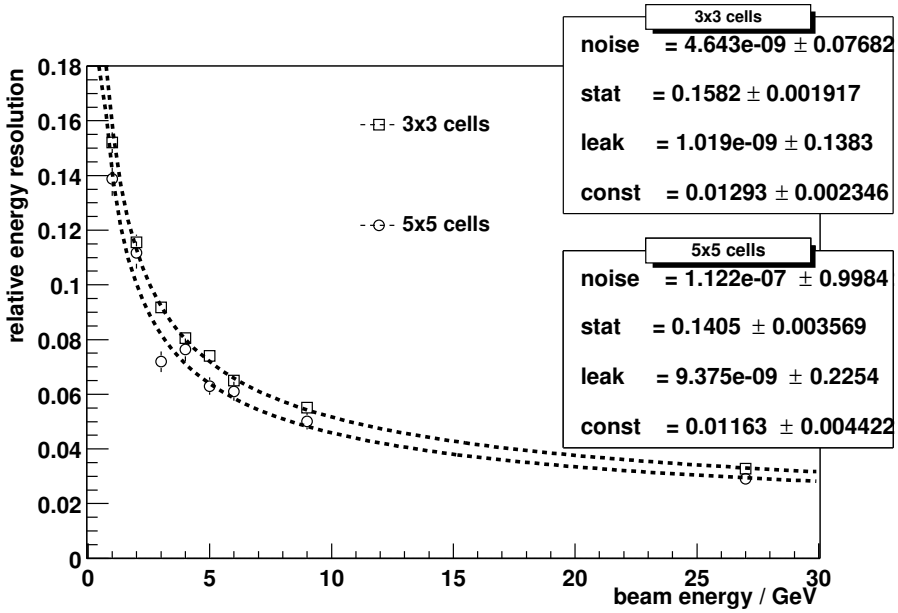

Figure 6.5: *Energy resolution of the detector for simulation data. For each energy the ratio of sigma to mean of the energy spectrum is plotted. The curves correspond to the fit results using all terms described in section 4.2.*

The statistical parameter is smaller than the one obtained from the testbeam, but comparable to the one observed in the gate length study (section 6.6). Additionally a constant term can be seen, which wasn't fitted for the testbeam data due to the limited energy range. The missing leakage term shows that even for high energies no longitudinal leakages are to be expected.

6.4 Fine scan

To test the position reconstruction and the uniformity of the energy reconstruction, a fine scan using the 3 mm hole was performed. The fine scan data was obtained by moving the detector in steps of 2.5 mm in x- and y-direction.

To test the uniformity of the energy reconstruction, the reconstructed energy was plotted against the x-position for all y-positions (left half of figure 6.6). To get a better estimation of the non-uniformities the relative difference from the mean is plotted. For 5×5 cells, the mean is taken for each y-position independently, because in y-direction the scan area was bigger than the fiducial volume, while for 3×3 cells it is calculated using all positions. This gives a nonuniformity of up to 2 % in x-direction for 5×5 cells and up to 3 % in x- and y-direction for 3×3 cells.

To be independent of the set position of the beam on the tagger, the position can be reconstructed with the tagger itself (see section 4.3). Using the corrected position reconstruction the tagger was divided in 2×2 mm^2 sized segments and then the uniformity analysis was applied to the calibration data (figure 6.7). This shows (except for $x = -10$ mm and $x = 7$ mm) deviations from uniformity of up to 2.5 % for 5×5 and 3 % for 3×3 cells. This result has to be used with care, because the resolution of the position reconstruction is of the order of the segment size used.

The non-uniformity at $x = -10$ mm is probably caused by a misscalibration of cell 15 (see figure A.3). The cause of the nonuniformity at $x = 7$ mm is not known. It is too narrow for a complete cell, but it could perhaps be some broken fibers.

To test the linearity of the position reconstruction, the reconstructed position is plotted against the position of the tagger relative to the beam (figure 6.8). This shows the basic position reconstruction to be linear within 0.8 mm and the corrected position reconstruction to be linear within 0.2 mm. The simulation shows a strong dependence of the reconstructed position on the electron energy (figure 6.9) which could result in non-linearities/non-uniformities of up to 0.3 mm. Because this effect is linear with the angle it could result in non-linearities/non-uniformities of up to 1.4 mm. This should be corrected for at ZEUS.

To test the resolution of the corrected position reconstruction, the width of the distribution at each position can be plotted (figure 6.10). This mean width is 1.20 mm in x-direction and 0.91 mm in y-direction. After correcting for the trigger width (3 mm hole) a resolution of 0.93 mm in x-direction and 0.51 mm in y-direction was obtained. From the simulation much smaller values are expected (figure 6.11), but it shows that the resolution improves with the energy.

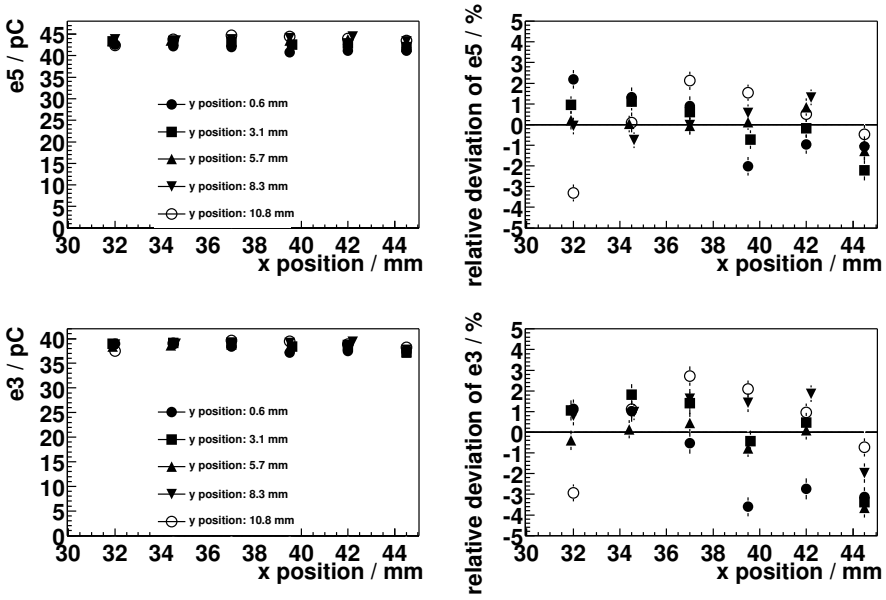

Figure 6.6: *Energy uniformity using the fine scan data. Reconstruction with* 5×5 *cells (upper row) and* 3×3 *cells (lower row). On the left the reconstructed energy is plotted against the position, on the right the relative deviation from the mean is plotted.*

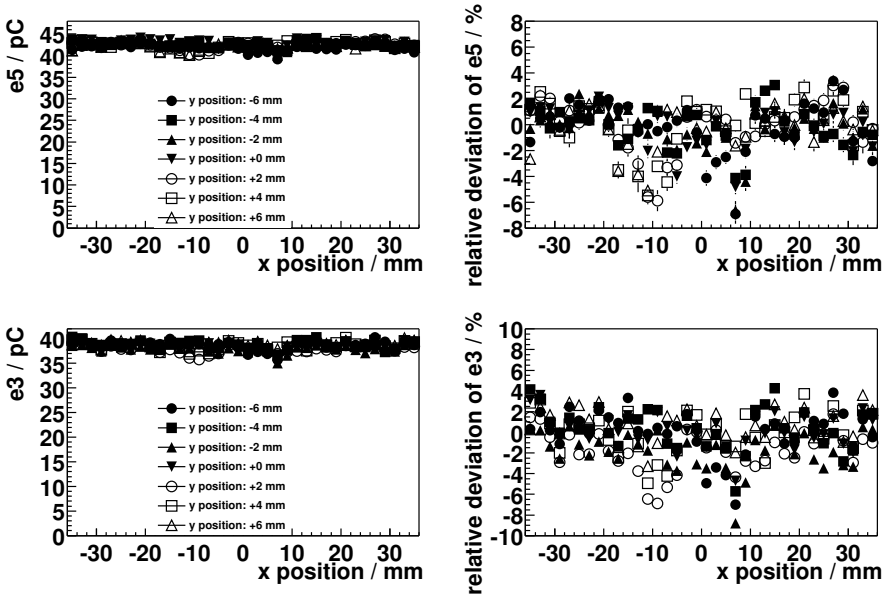

Figure 6.7: *Energy uniformity using the position reconstruction. For this plot the corrected position reconstruction has been used to seperate the calibration data into small pieces. In all other aspects it's the same as in figure 6.6.*

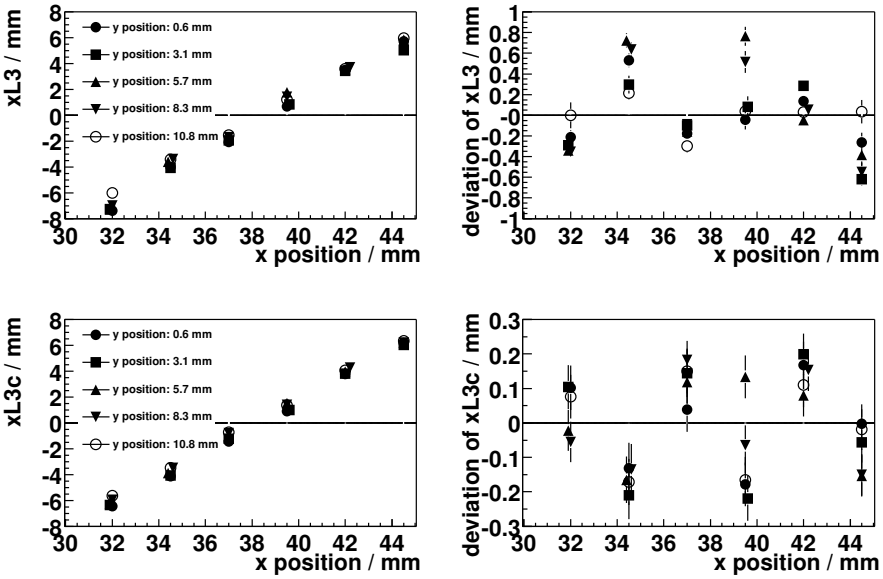

Figure 6.8: *Linearity of the basic (top) and corrected (bottom) position reconstruction. On the left the reconstructed position is plotted against the beam position, on the right the deviation from a fit with a straight line is plotted.*

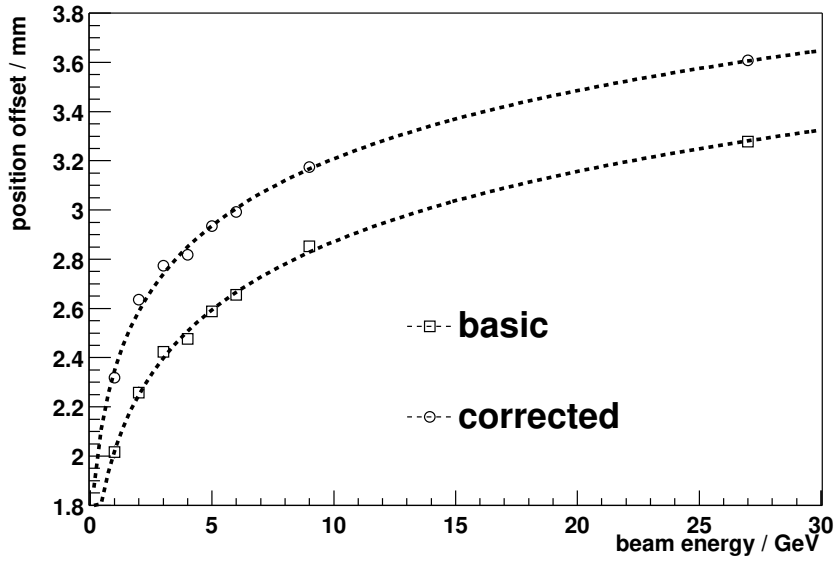

Figure 6.9: *Offset of the basic and corrected position reconstruction from the incident position for simulated data with a 5° incident angle. A logarithm has been fitted to the data.*

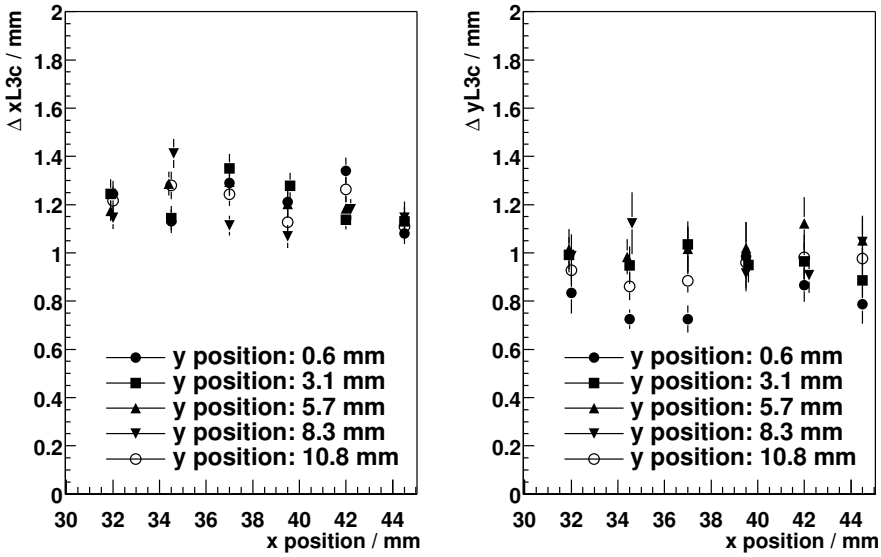

Figure 6.10: *Resolution in x- (left) and y-direction (right) of the corrected position reconstruction (3×3 cells) using a* 3 mm *hole. Plotted is the width of the distribution against the beam position.*

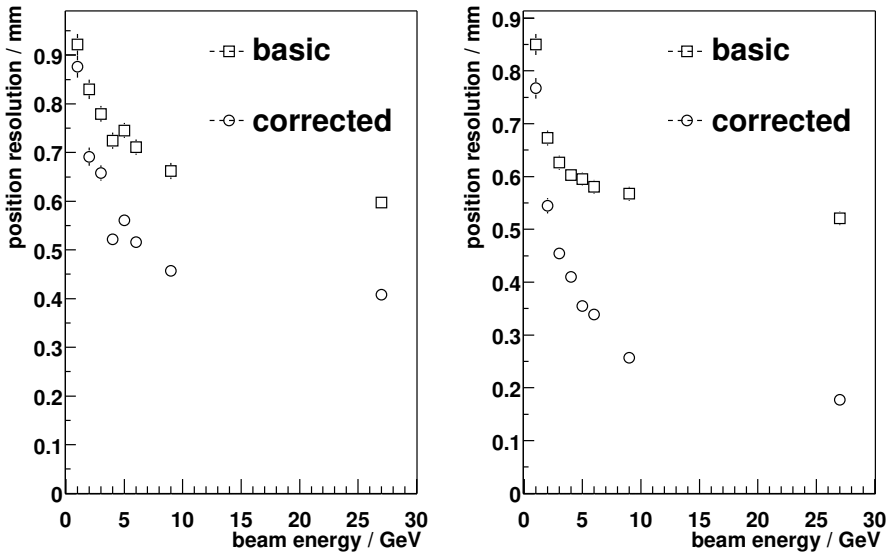

Figure 6.11: *Resolution in x- (left) and y-direction (right) of the basic and corrected position reconstruction for simulated data.*

6.5 Influence of incident angle

Most of the measurements have been made at an incident angle of 6°. To test the influence of the angle, energy scans at angles from 0° to 7° have been performed (see section 6.3). The electrons hit in the center of the detector using the finger counters T1 and T2 in coincidence. For the luminosity measurement the angles between 4° and 7° are important. For other measurements, smaller angles can occur.

For each angle the mean signal has been plotted against the energy. To this a straight line has been fitted. The slope of this fit can be used as gain factor. This gain factor shows a fall of 4.5 % and 2.5 % for 3×3 and 5×5 cells, respectively, if the angle is decreased from 3° to 7° (figure 6.12). This is an effect that would further decrease uniformity and should therefore be corrected at ZEUS.

Plotting the statistical parameter $\Delta E_{stat}/E$ of the resolution fit against the angle (figure 6.13) gives an estimate of how much influence the incident angle will have. In the range from 3° to 7° the resolution is almost independent of the angle, but for angles smaller than 2° it rapidly degrades. At ZEUS this decrease is only important for kinematic peak events.

6.6 Gate length study

The testbeam measurement has been done using an ADC gate length of 188 ns. At ZEUS a gate length of 70 ns will be used. To test the influence of the different gate length energy scans with the gate length 40, 60, 80 and 188 ns have been performed

Plotting the statistical parameter $\Delta E_{stat}/E$ of the resolution fit against the gate length (figure 6.14) shows that the resolution increases as the gate length continues to decrease. This is rather surprising since the gate is to short to contain the complete pulse (figure 6.15). For ZEUS this implies that at least the 5×5 resolution will be one percent better than at the testbeam.

6.7 Summary of testbeam measurements

Except for one cell the detector has been successfully calibrated with the newly devised calibration method.

The energy reconstruction is linear within ±0.8%, resp. ±1.3% for 3×3 resp. 5×5 cells. It has a resolution of

$$17.0\%/\sqrt{E} \oplus 15.7\%/E \quad \text{for } 5 \times 5 \text{ cells} \tag{6.5}$$

$$18.4\%/\sqrt{E} \oplus 12.4\%/E \quad \text{for } 3 \times 3 \text{ cells} \tag{6.6}$$

where E is given in GeV. Due to the shorter gate length the resolution will probably be 1% better at ZEUS. For very small angles the resolution might degrade by several percent. The non-uniformity is less than ±3% and ±2.5%, respectively. Due to the signal height changing with the angle an additional non-uniformity or non-linearity of up to ±2.5% could happen which has to be corrected using software.

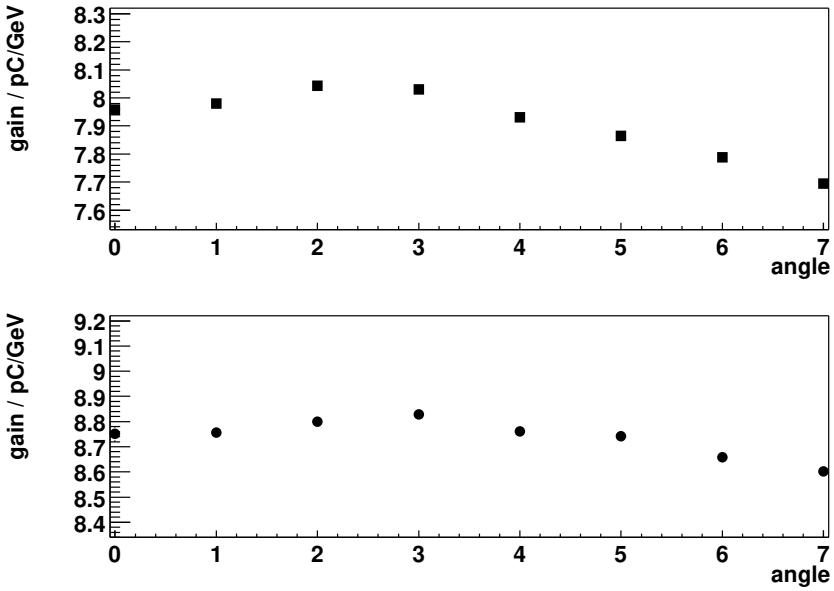

Figure 6.12: *Gains for different incident angles for the reconstruction in* 3×3 *cells (top) and* 5×5 *cells (bottom). For each angle the reconstructed energy was plotted against the beam energy and fitted with a straight line. The slopes of these lines are taken as gain factors and are plotted against the angle.*

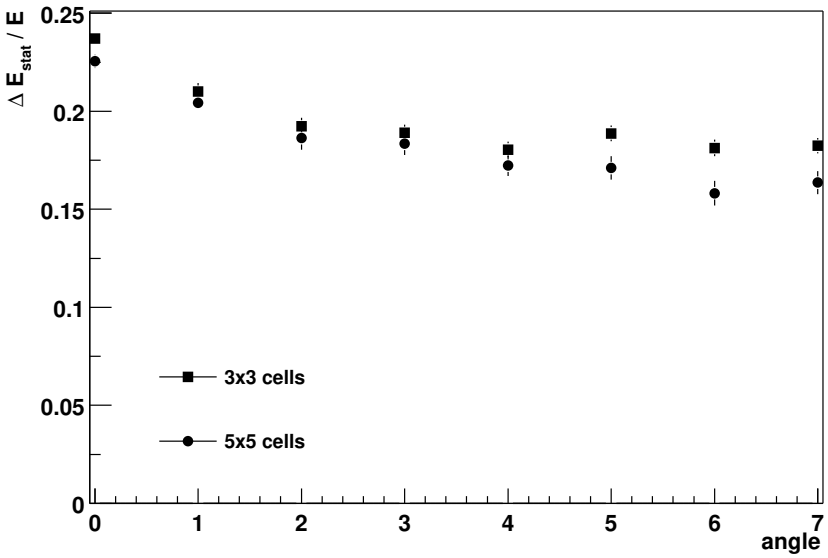

Figure 6.13: *Statistic parameter of energy resolution fit for different incident angles. For each angle the relative energy resolution has been plotted against the energy and fitted using equation 5.1. The* $\Delta E_{stat}/E$ *parameter of this fit was plotted against the angle.*

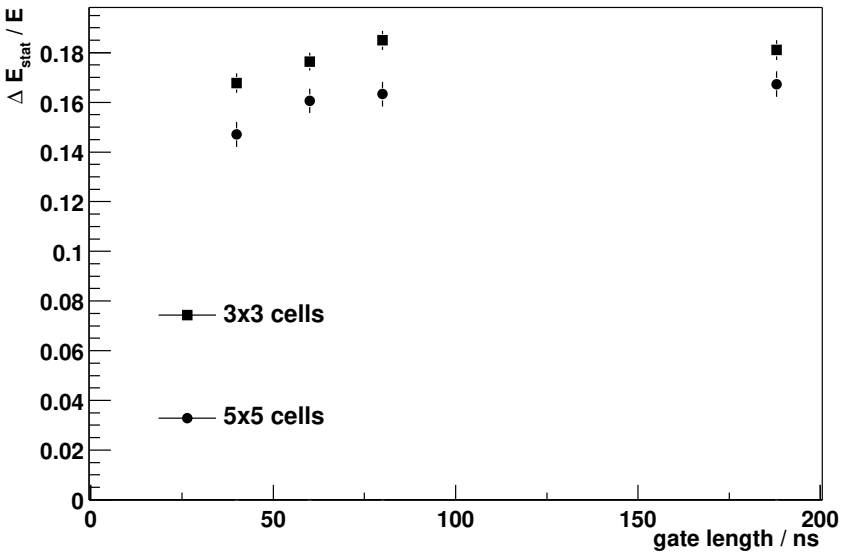

Figure 6.14: *Statistic parameter of energy resolution fit for different gate length. For each gate length the relative energy resolution has been plotted against the energy and fitted with equation 5.1. The $\Delta E_{stat}/E$ parameter of this fit was plotted against the gate length.*

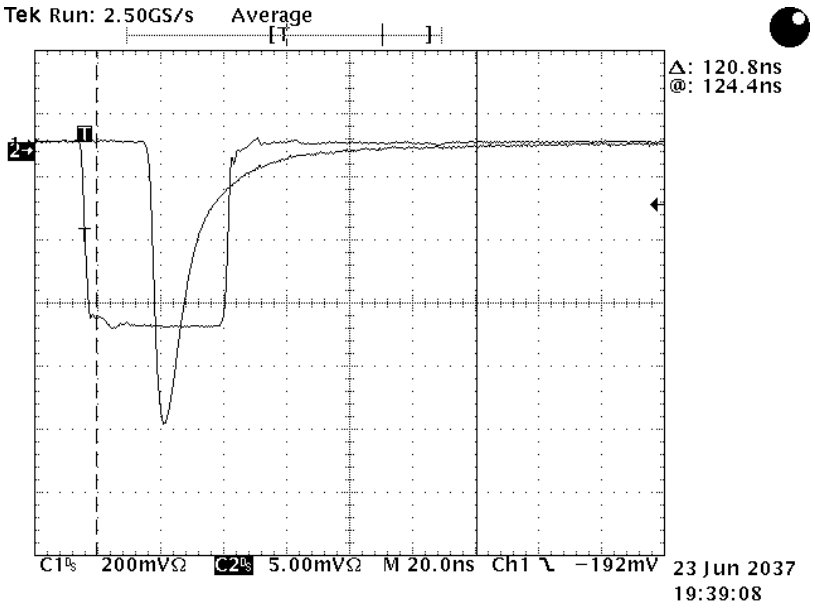

Figure 6.15: *Pulse shape and 40 ns gate. The pulse was recorded using the complete wire between PMT and ADC used at the testbeam ($\sim$ 40 m). The gate length was modified by moving the rising edge of the gate.*

At 5 GeV the corrected position reconstruction was shown to be linear within ± 0.2 mm and to have a resolution of 0.93 mm in x- and 0.51 mm in y-direction. The simulation shows that for bigger energies the resolution should improve significantly, but only if the influence of incident angle and energy are compensated.

Chapter 7

Summary

The detector has been successfully built and tested with 1–6 GeV electrons and is ready for installation at ZEUS. A Monte Carlo simulation of the detector has been developed. The newly devised calibration method has been successfully applied.

The energy reconstruction was shown to be linear within $\pm 0.8\%/\pm 1.3\%$ for $3 \times 3/5 \times 5$ cells. Its relative energy resolution is

$$17.0\%/\sqrt{E} \oplus 15.7\%/E \quad \text{for } 5 \times 5 \text{ cells} \tag{7.1}$$

$$18.4\%/\sqrt{E} \oplus 12.4\%/E \quad \text{for } 3 \times 3 \text{ cells} \tag{7.2}$$

where E is given in GeV. The testbeam experiment had an ADC gate length of 188 ns. Due to the shorter gate length of 67 ns the resolution will probably be 1% better at ZEUS. For very small angles of incidence ($< 2°$) the resolution might degrade by several percent.

Simulation runs have been done for energies of 1–27 GeV giving the better resolution

$$14.1\%/\sqrt{E} \oplus 1.2\% \oplus \Delta E_{noise}/E \quad \text{for } 5 \times 5 \text{ cells} \tag{7.3}$$

$$15.8\%/\sqrt{E} \oplus 1.3\% \oplus \Delta E_{noise}/E \quad \text{for } 3 \times 3 \text{ cells} \tag{7.4}$$

Possible reasons for this difference include the long gate length and the low PMT gain. For the prototype the simulation could reproduce the energy resolution.

At 5 GeV the corrected position reconstruction was shown to be linear within ± 0.2 mm and to have a resolution of 0.93 mm in x- and 0.51 mm in y-direction. The simulation shows that for bigger energies the resolution should improve significantly.

The simulation was shown to be accurate for the energy reconstruction except for the effects by electronic noise. For the position reconstruction the simulation showed a much smaller resolution, which could be caused by electronic noise.

Appendix A

Calibration data

In this appendix a complete listing of the calibration data is given for the prototype and the complete detector. For each cell the high voltages and the results from the first and second calibration step are printed.

For the prototype the signal is measured in ADC counts with 4 ADC counts being about 1 pC. The high voltages have been adjusted using the signal of the LED system.

For the complete detector the signal is measured directly in pC. The high voltages have been adjusted by applying the first calibration step two times before and changing the high voltages each time to get about 8 pC / GeV. The calibration target of the calibration printed here was that the mean of the calibration constants is 1 for the central cells.

cell	PMT	HV/V	n_1	c_1	n_2	c_2
10	4L30EK	960	5669	0.0636	104	0.0568
11	EA0495	870	5109	0.0707	295	0.0621
12	BB0380	940	5220	0.104	295	0.0955
13	BB0214	890	3201	0.126	173	0.121
14	BB0414	960	6580	0.0637	81	0.0562
15	4K18EJ	—	0	0.00	0	0.00
20	4L22EA	940	5737	0.0890	336	0.0777
21	5H23BA	920	4928	0.108	76	0.0989
22	BB0444	960	3250	0.139	36	0.124
23	BB0213	990	6314	0.0955	90	0.0865
24	BB0451	900	4458	0.105	153	0.101
25	BB0372	970	5934	0.0642	105	0.0615
30	5B01AK	915	3969	0.184	586	0.185
31	BA0114	825	3821	0.135	30	0.126
32	4K25EK	985	10868	0.0814	64	0.0705
33	BB0377	885	4926	0.120	54	0.109
34	BB0452	945	4112	0.148	92	0.138
35	BB0392	950	5078	0.0699	230	0.0684
40	5H08BJ	840	3813	0.170	265	0.166
41	BB0421	945	5768	0.0944	36	0.0840
42	BB0389	950	8495	0.0641	114	0.0582
43	BB0376	890	4257	0.126	131	0.118
44	4M06EH	850	4147	0.147	105	0.133
45	BB0379	960	4774	0.0930	194	0.0922
50	BB0454	970	4957	0.125	89	0.115
51	4M06EB	900	4719	0.112	248	0.0916
52	BB0373	975	3510	0.116	301	0.109
53	BB0395	915	5304	0.101	249	0.0888
54	BB0447	900	2540	0.176	113	0.162
55	BB0428	990	5635	0.0862	25	0.0790

Table A.1: *High voltage settings and calibration constants from first and second step of calibration for the prototype detector. n_i denote the number of calibration events in step i and c_i the calibration constants, i.e. the ratio of desired signal to measured signal. The high voltage was set so that the LED signals of all cells were the same.*

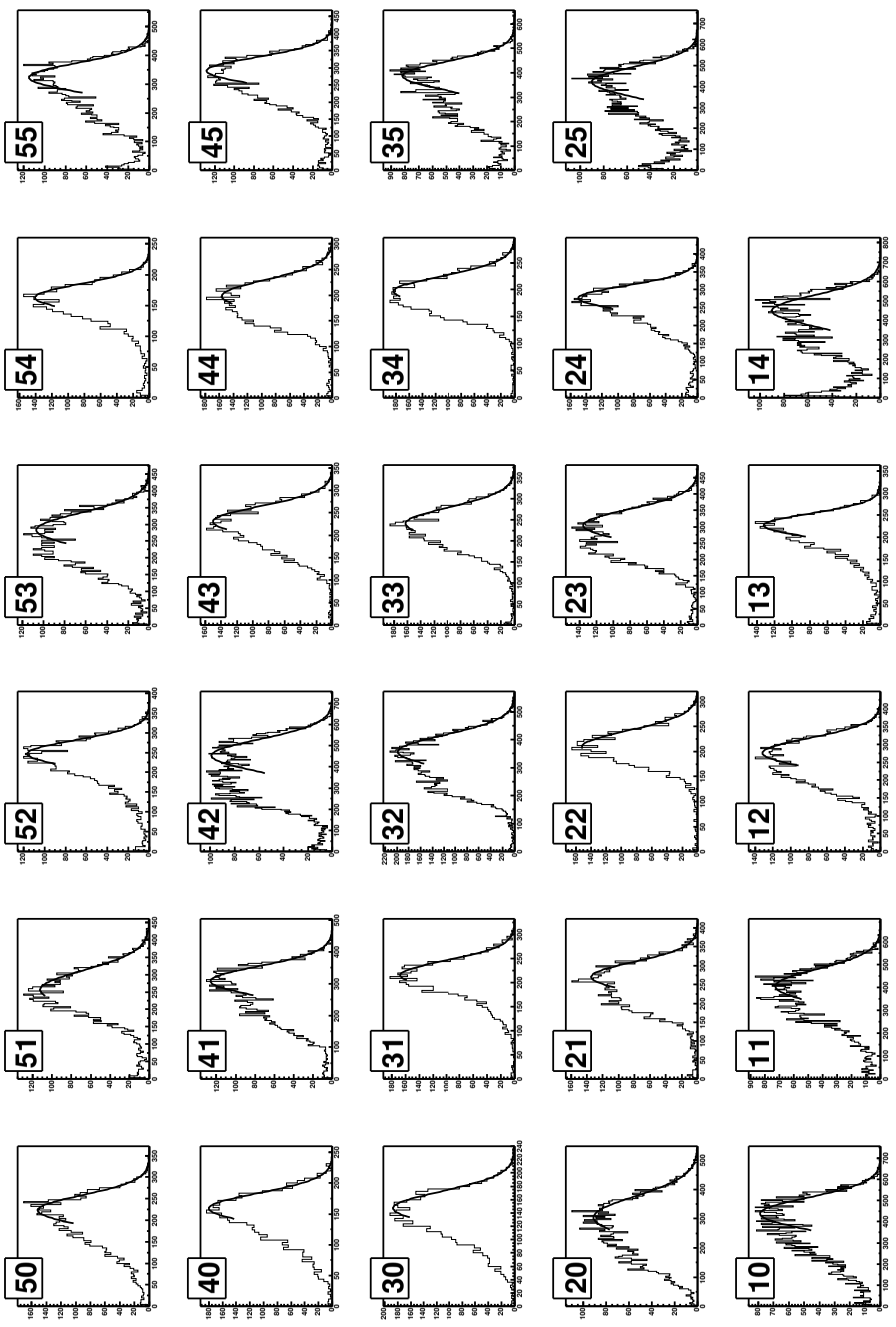

Figure A.1: *Calibration spectra for the first calibration step of the prototype detector.*

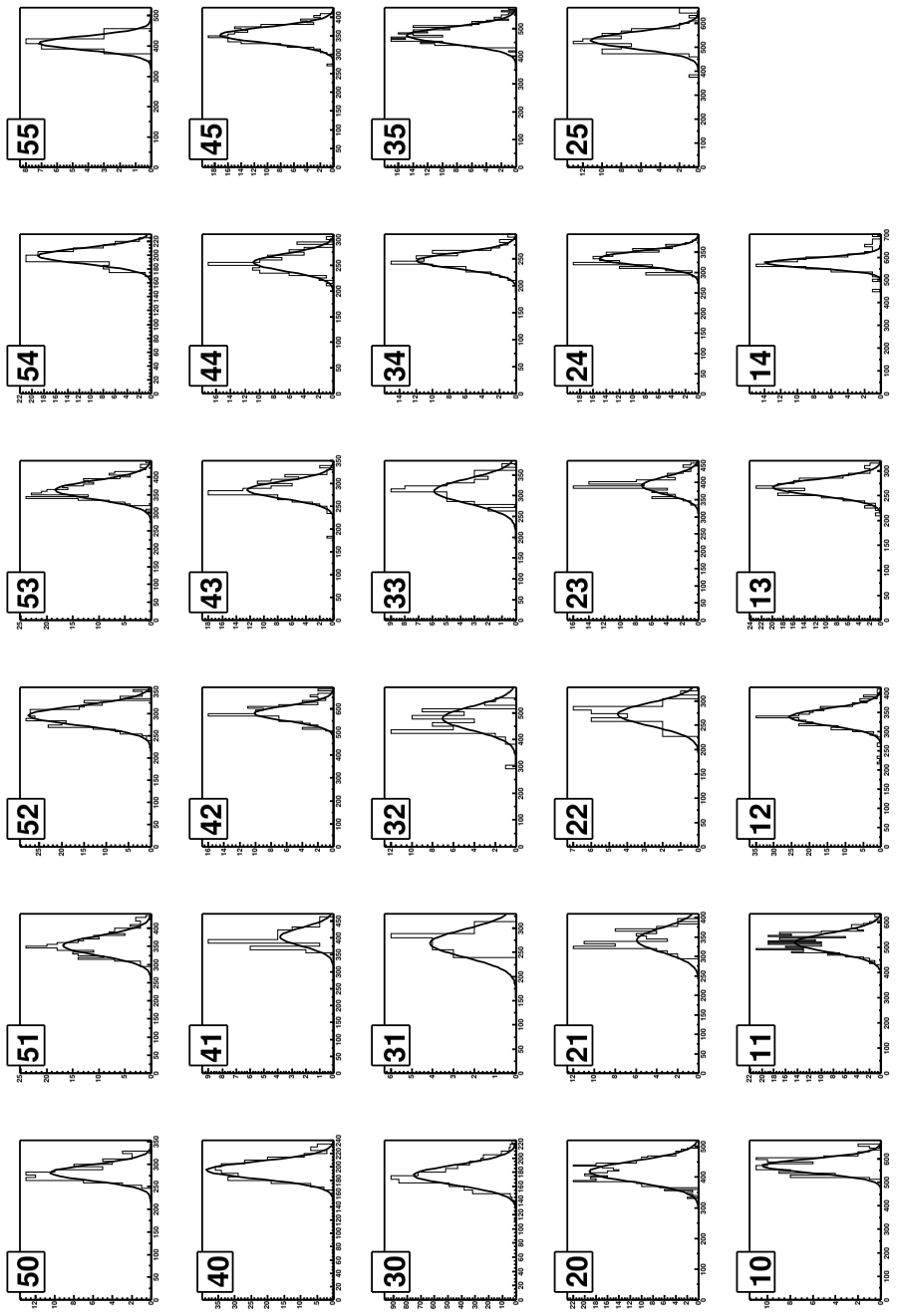

Figure A.2: *Calibration spectra after cuts of the second calibration step of the prototype detector.*

cell	PMT	HV/V	n_1	c_1	n_2	c_2
10	BA0435	640	11262	0.904	3760	1.08
11	BA0130	727	16603	0.952	3852	1.00
12	BA0510	690	15656	0.894	4233	1.01
13	BA0297	649	15534	0.901	4466	1.00
14	BA0305	632	11961	0.961	3301	1.09
15	BA0100	698	14976	0.867	4595	0.980
16	BA0493	652	11644	0.997	3670	1.15
20	BA0108	727	16283	0.822	3862	0.958
21	BA0177	692	16984	0.917	1589	0.960
22	BA0193	658	19810	0.894	1684	0.943
23	BA0507	664	18320	0.891	1494	0.942
24	BA0275	647	15380	0.907	1504	0.986
25	BA0106	669	16749	0.915	1871	0.983
26	BA0446	721	16386	0.890	2143	0.966
30	BA0496	668	17689	0.868	4331	1.00
31	BA0498	678	19995	0.842	1925	0.914
32	BA0174	686	20092	0.846	1857	0.927
33	BA0108	700	18894	0.828	1675	0.879
34	BA0088	673	16095	0.894	1496	0.959
35	BA0081	690	18293	0.888	2622	0.979
36	BA0512	713	21581	0.881	3075	0.972
40	BA0202	681	12782	0.904	3224	1.04
41	BA0506	699	14343	0.846	1278	0.896
42	BA0503	698	16018	0.827	1379	0.876
43	BA0184	659	12830	0.876	916	0.948
44	BA0129	694	14403	0.864	2313	0.940
45	BA0504	640	9877	1.41	774	1.46
46	BA0179	676	17934	0.921	2038	0.973
50	BA0519	680	9133	0.891	3093	1.03
51	BA0115	689	10302	0.890	2531	0.991
52	BA0104	746	11789	0.899	2746	0.958
53	BA0124	768	10606	0.890	2325	0.953
54	BA0166	706	10451	0.857	2640	0.943
55	BA0127	673	11249	0.854	3207	0.952
56	BA0497	670	12438	0.907	3061	0.974

Table A.2: *High voltage settings and calibration constants from first and second step of calibration for the first part of the tagger (cells 10–56). The high voltage was determined by applying the first calibration step two times befofe.* n_i *denote the number of calibration events in step* i *and* c_i *the calibration constants, i.e. the ratio of desired signal to measured signal.*

cell	PMT	HV/V	n_1	c_1	n_2	c_2
17	BA0492	655	13588	0.850	4270	0.940
18	BA0221	675	13649	0.780	4260	0.908
19	BA0508	699	10614	0.878	2835	0.970
1a	BA0282	677	9276	0.931	2651	1.06
1b	BA0182	688	10179	0.957	2673	1.03
1c	BA0161	687	8761	0.906	2348	1.00
1d	BA0502	708	11545	0.891	1780	0.889
27	BA0447	664	19181	0.870	3958	0.978
28	BA0171	672	16345	0.864	1638	0.944
29	BA0122	761	16594	0.816	1803	0.843
2a	BA0526	671	14585	0.907	1297	0.977
2b	BA0128	691	15560	0.893	1593	0.932
2c	BA0205	710	13049	0.847	1379	0.919
2d	BA0101	691	8911	0.892	2396	0.971
37	BA0499	666	24073	0.860	3772	0.948
38	BA0136	691	22451	0.844	2802	0.903
39	BA0084	710	17972	0.864	1589	0.904
3a	BA0490	661	17303	0.910	1751	0.973
3b	BA0206	729	20678	0.909	2099	0.931
3c	BA0487	663	14992	0.897	1306	0.967
3d	BA0287	642	11780	0.876	3330	0.954
47	BA0086	655	16711	0.900	2040	0.985
48	BA0175	697	17197	0.807	2080	0.877
49	BA0270	674	15283	0.869	1451	0.902
4a	BA0188	659	13964	0.892	1259	0.944
4b	BA0196	681	12656	1.03	909	1.08
4c	BA0480	707	12503	0.880	1250	0.960
4d	4M06EH	720	10410	0.934	2373	0.981
57	BA0255	683	10474	0.886	2925	0.976
58	BA0500	718	13193	0.764	3588	0.845
59	BA0494	674	11055	0.874	2952	0.977
5a	BA0264	660	9953	0.904	2241	0.979
5b	BA0529	662	10943	0.950	2576	1.03
5c	BA0505	683	8902	0.906	1778	0.992
5d	4K25EK	751	7863	0.793	2027	0.828

Table A.3: *High voltage settings and calibration constants from first and second step of calibration for the second part of the tagger (cells 17–5d). Continuation of table A.2.*

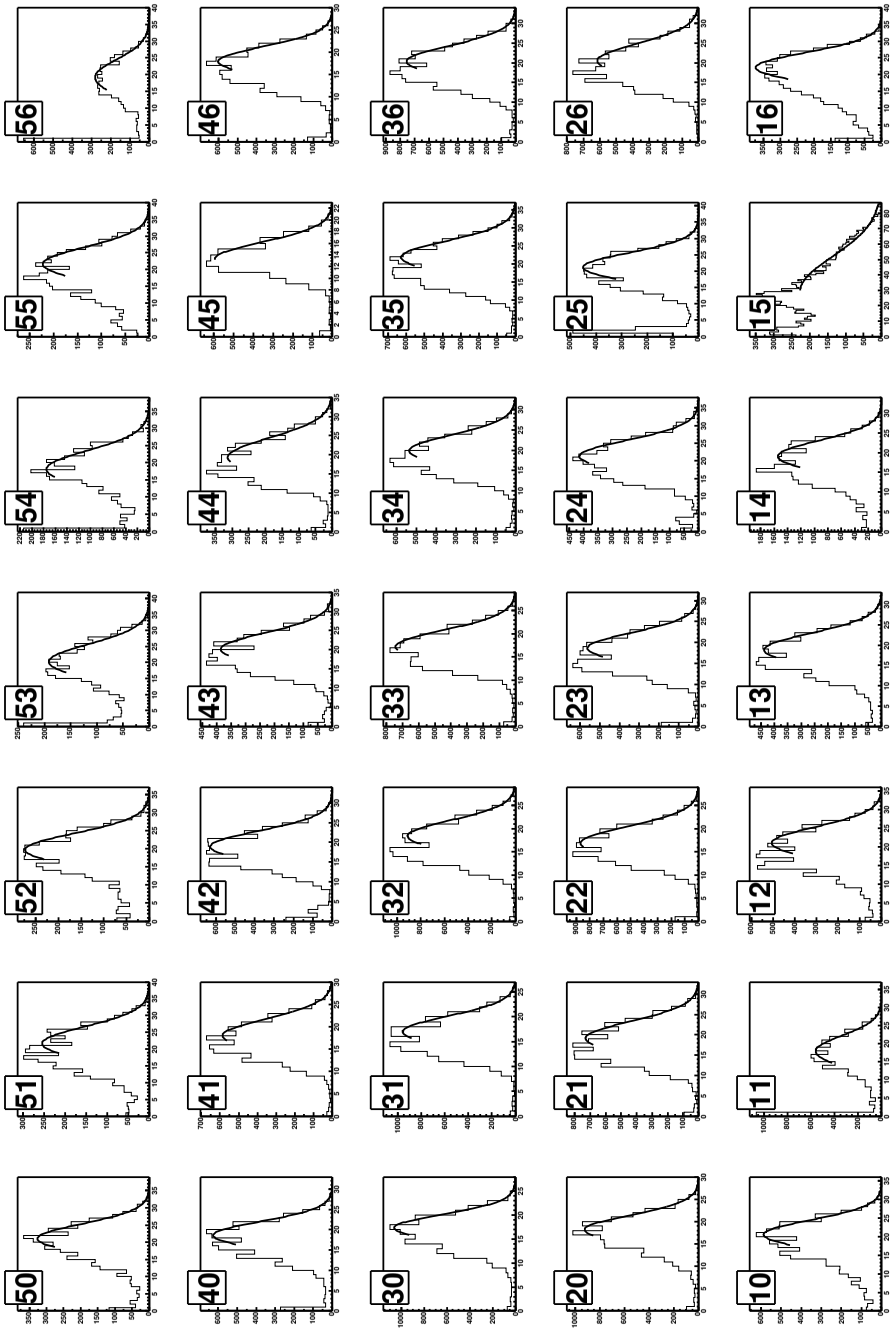

Figure A.3: *Calibration spectra of the first part of the tagger (cells 10–56) for the first calibration step.*

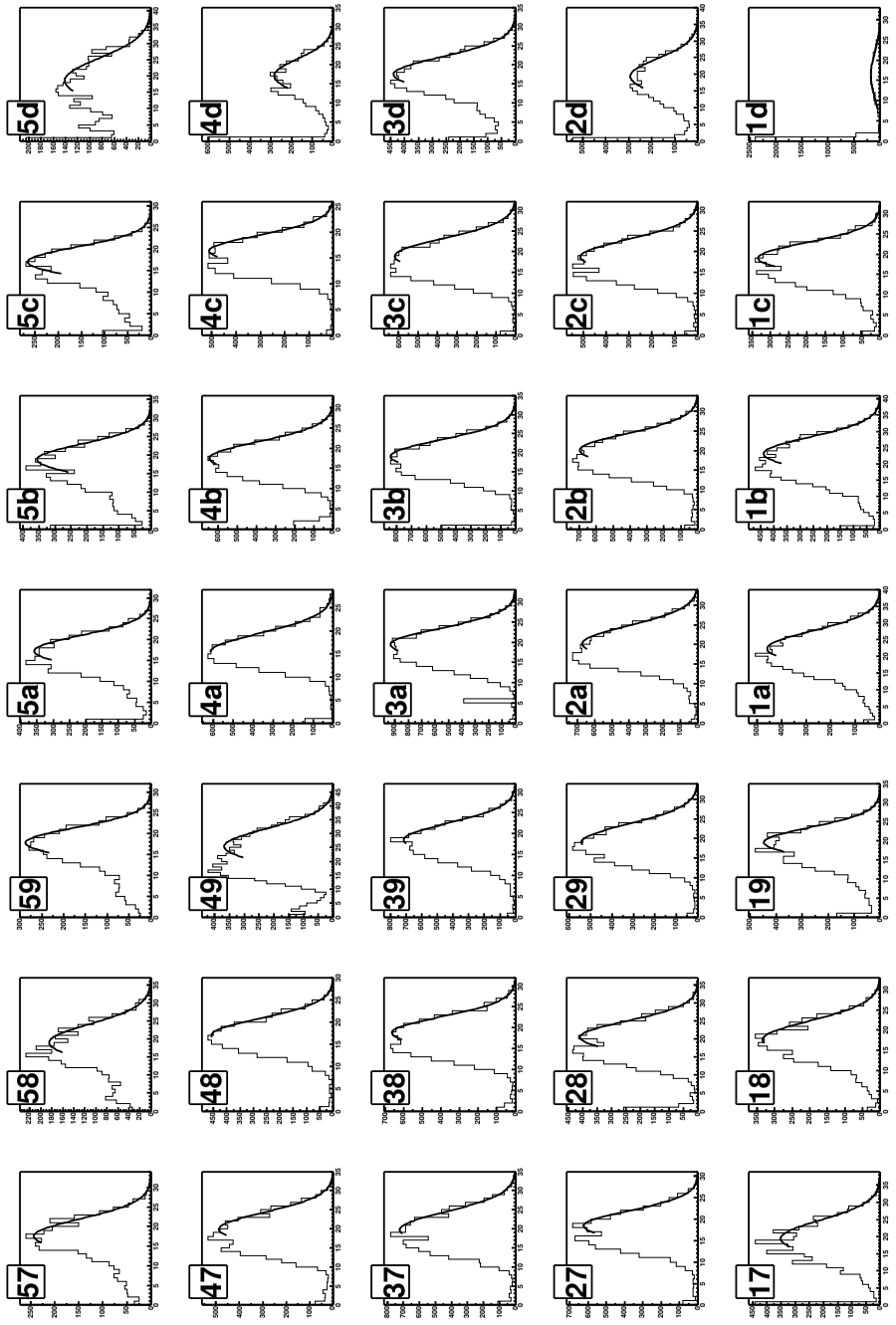

Figure A.4: *Calibration spectra of the second part of the tagger (cells 17–5d) for the first calibration step.*

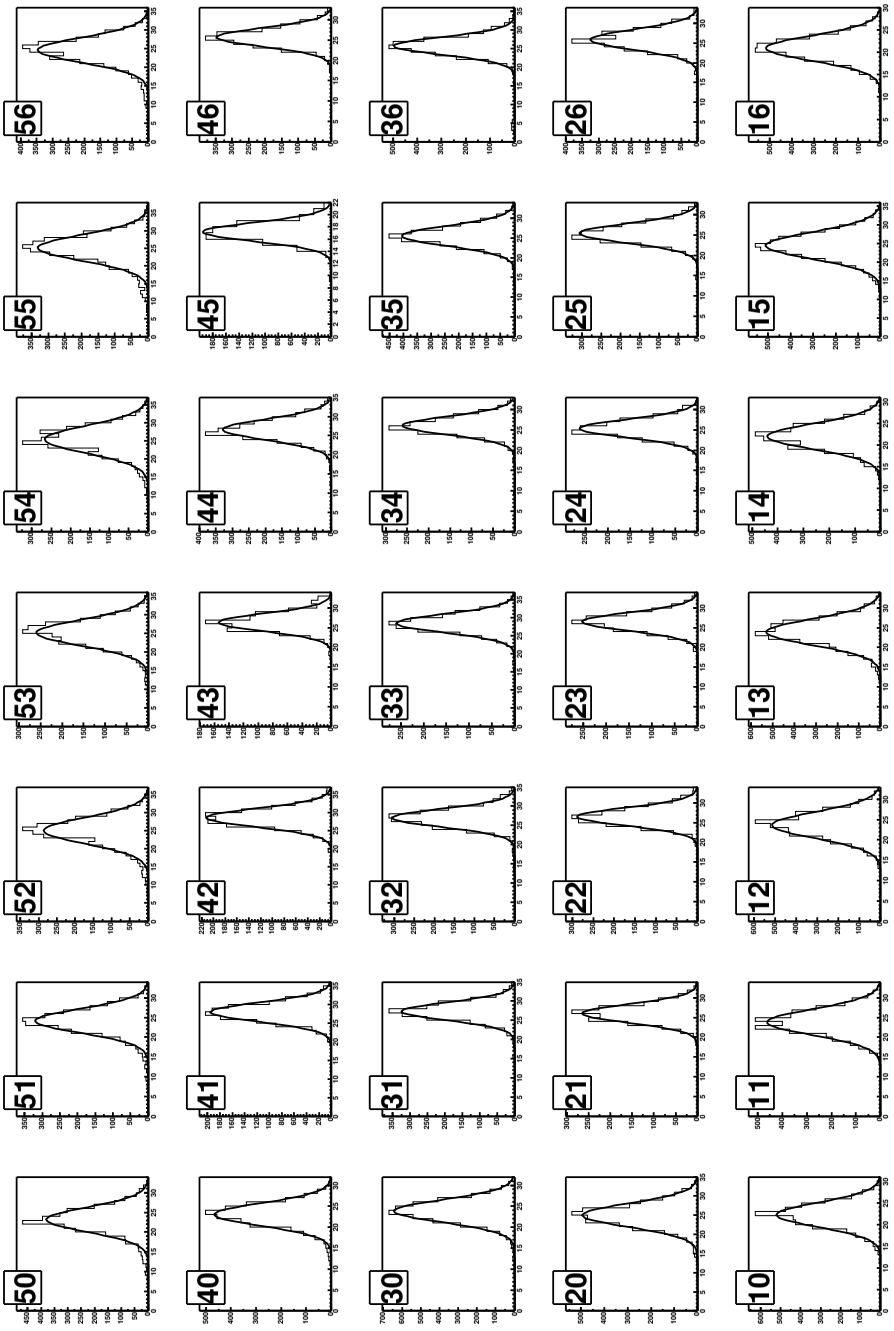

Figure A.5: *Calibration spectra of the first part of the tagger (cells 10–56) for the second calibration step.*

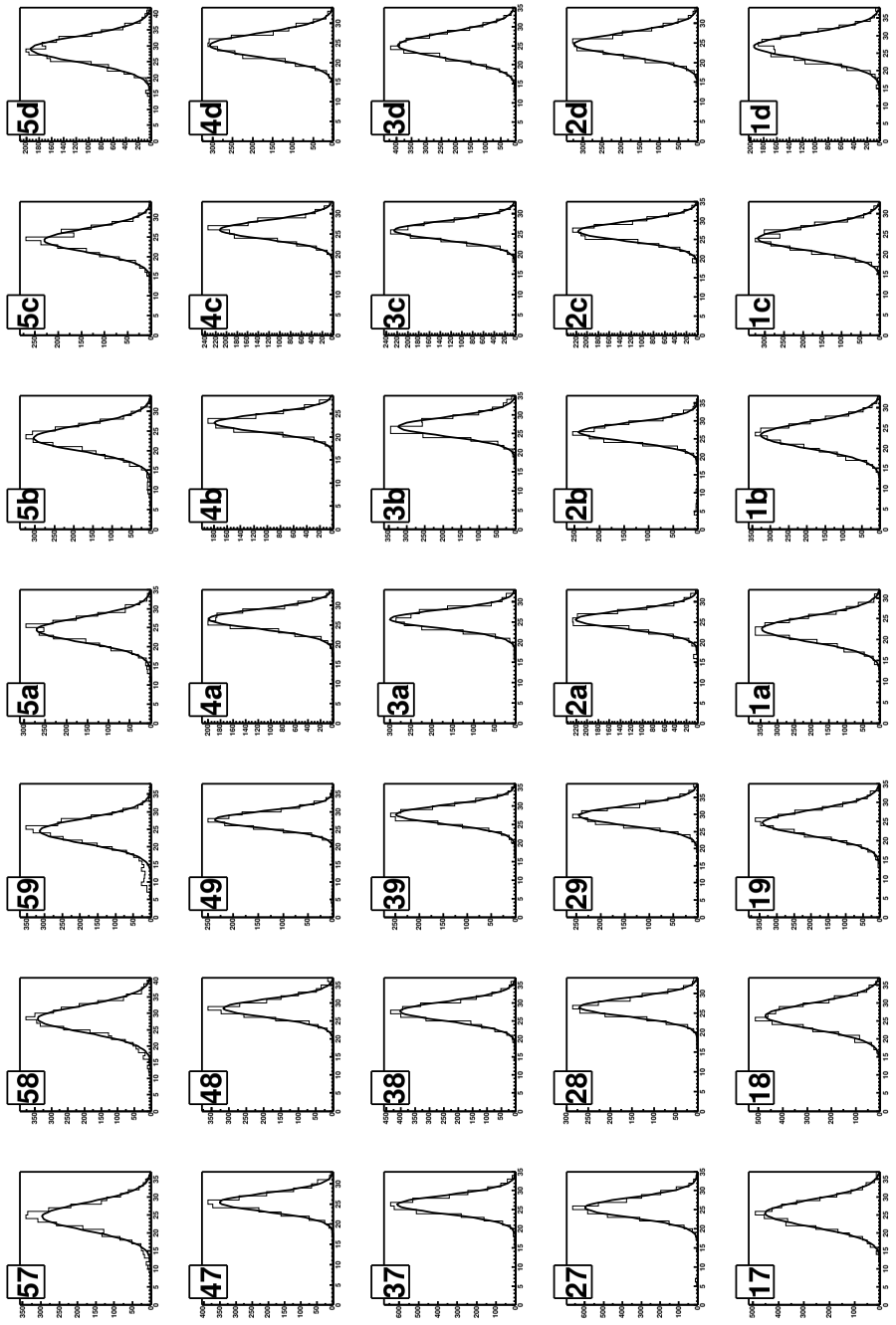

Figure A.6: *Calibration spectra of the second part of the tagger (cells 17–5d) for the second calibration step.*

Appendix B

Software documentation

For this thesis I developed three software programs:

- The Monte Carlo simulation
- The root macro doing all reconstructions and generating the root tree containing all data.
- The root macro analysing the data.

For each program I will give a brief explanation on how to use it. All these programs run non-interactively, which means you have to start them with the correct parameters and then they do their work creating the files containing the desired data.

B.1 The Monte Carlo simulation

This program reads all parameters from standart input. Therefore it is best to create a file containing the parameters and then to start the program with this file as standart input. The program furthermore needs a file named `fort.12` in the current directory containing the PEGS4 data. It will then create a file named `fort.80` in the current directory, containing the simulated signal responses.

The parameters file might look like this:

```
TCAL-RANDOM        10.0
TCAL-G_MIN          0.010
TCAL-E_MIN          0.010
TCAL-START_X       -4.25
TCAL-START_Y       -1.2
TCAL-STOP_X         4.25
TCAL-STOP_Y         1.2
TCAL-CHARGE        -1.0
TCAL-ANGLE          0.0
TCAL-SUMMARY        1.0
TCAL-UNIT          80.0
TCAL-EVENTS      2500.0
TCAL-ENERGY      9000.0
****-********       0.0
```

The meaning of these parameters is:

RANDOM This is the random seed.

G_MIN This is the cutoff energy for photons.

E_MIN This is the cutoff energy for electrons.

START_X This is the minimum allowed x-coordinate (the center of the tagger is at $(0, 0)$).

START_Y This is the minimum allowed y-coordinate.

STOP_X This is the maximum allowed x-coordinate.

STOP_Y This is the maximum allowed y-coordinate.

CHARGE This is the charge of the incident particle.

ANGLE This selects between the fixed angle of 5° and random angles needed for the simulation of ^{60}Co-measurements.

SUMMARY The number of incident particles to sum over for one event.

UNIT This is the number of the output file.

EVENTS This is the number of particles to insert.

ENERGY This is the energy of the incident particle.

B.2 The treebuilder program

The treebuilder has some parameters compiled in (basically the parameters determening the type and amount of data written). The parameters directly determening the runs to use and the file to write to are given as command line parameters. In order to generate the tree it needs the testbeam, resp. simulation data installed under `~/data/beam/testbeam<X>/`, resp. `~/data/egs4/<Y>/`. `<X>` is `1` for the prototype detector and `2` for the final detector. `<Y>` is `prototype` for the prototype detector and `detector` for the final detector.

The compile time options are set as definitions in the file `loadTree.h`:

DROPRAW If this is defined the raw data will not be stored in the ROOT-file.

DROPCAL If this is defined the calibrated data will not be stored in the ROOT-file.

DROPNEXT If this is defined information about the energy in the neighbouring cells is not stored.

FITFORPOS If this is defined the program will try to fit a Gaussian curve to the signal distribution and thereby try to determine energy and position of the incident particle (very slow and not usefull).

CELLS_X This has to be 6 for the prototype detector and 14 for the final detector.

The program takes a number of command line parameters:

1. The name of the ROOT-file in which to store the tree.
2. The mode with which to open the ROOT-file.
3. The name of the tree to create.
4. The title of the tree to create.
5. the type of data to use (`tb1`/`tb2`/`mc`).
6. Selection parameters indicating which subset of the data to use.

For simulation runs the selection parameters consists of a flags field indicating the energies to use and the number of data files to read.

For the 1st testbeam the selection parameters consists of a selection flags field and the calibration number. For a run to be used its selection flags must be contained in the selection flags parameter.

For the 2nd testbeam the selection parameters consist of a use, a nominal and a position switch, and high voltage and intention flags. The switches require the corresponding flag to be set for the run. The flag fields contain the high voltages/measurement types which are included.

The following branches are contained in all trees:

raw The uncalibrated energy in each cell.

cal The calibrated energy in each cell.

xMax,yMax,zMax The index of the central cell.

xMaxC,yMaxC,zMaxC The index of the cell with maximum energy.

xMaxS,yMaxS,zMaxS The index of the row/column with maximum energy.

xMaxM,yMaxM,zMaxM The index of the cell hit according to the global position reconstruction.

xCen3,yCen3 The center of the 3×3 reconstruction region.

xCen5,yCen5 The center of the 5×5 reconstruction region.

xV3,yV3,xV5,yV5,xVAll,yVAll Energy deposited in the different rows/columns of the reconstruction region.

e1r,e1 Uncalibrated/calibrated energy deposited in the central cells.

e3,e5,eAll Energy in the different reconstruction regions.

eN1,eN2,eN3,eN4 Energy in the cells with the next to maximum energy.

eST,eSB,eSR,eSL Energy in the cells above, below, right and left of the central cells.

xL3,yL3,xL5,yL5,xLAll,yLAll Reconstructed position using the position reconstructions in the different reconstruction regions.

xL3d,yL3d Distance to the central cell using the basic 3×3 position reconstruction.

xL3c,yL3c Corrected position reconstruction.

sL3,sL5,sLAll Shower size in the different reconstruction regions.

dist0 RMS of the shower using the center of the tagger as mean.

f3C,f3MX,f3MY,f3SX,f3SY Fit parameters for fitting a gaus in the 3×3 reconstruction region fitting for x and y at once.

fCX3,fMX3,fSX3,fCY3,fMY3,fSY3 Fit parameters for fitting a gaus in the 3×3 reconstruction region fitting for x and y seperately.

fCX5,fMX5,fSX5,fCY5,fMY5,fSY5 Fit parameters for fitting a gaus in the 5×5 reconstruction region fitting for x and y seperately.

run The run number.

event The event number.

inE The energy of the electron in MeV.

sel3,sel5 Wether this event lies in the fiducial volume of the 3×3 or 5×5 reconstruction region.

The simulation data contain the following additional branches:

detX,detY,detZ The size of the detector.

fibR The radius of the fibers.

holR The radius of the holes.

delX,delY The spacing between the fibers.

fibCX,fibCY,fibCZ The number of fibers in the different directions (z means number of segmentations.

secSX,secSY,secNX,secNY Internal data useful for debugging the simulation.

inReg The region in which the particle started.

inX,inY,inZ The starting position of the particle.

inCosX,inCosY,inCosZ The cosines of the starting direction of the particle.

inCharge The charge of the starting particles.

regE The energy deposited in the different simulation regions.

fibE The energy deposited in the different fiber segments.

The testbeam data of the prototype detector contains the following additional branches:

time The timestamp of the run.

data,ped The adc values read before and after pedestal correction.

tr1h,tr1v,tr2h,tr2v The signal in the triggers.

cellX,cellY The position of the cell targeted.

posX,posY The position of the tagger.

trigX,trigY The size of the trigger in x- and y-direction.

sflags The selection flags.

The testbeam data of the final detector contains the following additional branches:

data The signals read for the different adc channels.

trS1,trS2,trS3,trT1,trT2 The signal in the triggers.

infUse Wether this run contains usable data.

infTrig Flags indicating which of the triggers where used.

infTLT The third level trigger used.

infI The current in the magnet controlling the energy of the beam. This is 37.4 times the beam energy in GeV.

infXSet,infYSet This is the set position of the tagger in mm.

infXRead,infYRead This is the read back position of the tagger (*not* in mm).

infSysLed This indicates wether the old or the new led system was used.

infILed This is the current of the LED in mA.

infCol This is the collimator used.

infAngle This is the incident angle.

infGate This is the gate length in ns.

infHV This is the HV setting used.

infIntent This is the type of measurement made.

cellX,cellY This is the cell targeted with the trigger.

selNom This indicates wether all fields have nominal values.

selLED This indicates wether this is an LED run.

B.3 The analysis program

The analysis program I will describe here has been used for nearly the complete analysis in this thesis. Although its functionality is basically quite simple, its very powerful and requires considerable amount of programming to achieve.

The program cuts on a number of conditions. Then it seperates the remaining events according to the value of one or two seperation variables. For each of these event groups it creates a histogram, fills it with the values of another variable for these events and then fits a Gaussian curve to it. The resulting mean, sigma, sigma/mean values are plotted against the first seperation variable and then arbitrary functions are fitted to these plots. If a second variable is available the fit parameters are plotted against the values of the second seperation variable. All plots are stored for later use. Also most of the event list are stored, to allow further analysis of the data.

The program is totally controlled via command line parameters. The mandatory parameters are:

1. An identifier for the ROOT file containing the tree to use.
2. The name of the ROOT file to write the results to.
3. The mode with which to open the output ROOT file.
4. The prefix to use for the name of all objects created.
5. The variable to use for plotting.
6. The kind of variable this is:

   0 energy

   1 x position

   2 y position

   3 other

   This information is used for determening the limits of the histogram and the fits.

After the mandatory parameters any number of optional parameters can be used. The optional parameters consist of a character indicating the type of parameter and a value the parameter is set to. The order of these parameters is important. The options are:

a Do a fiducial volume cut.

c Do an arbitrary cut.

d Do a fiducial volume cut using the position reconstruction.

e Do a cut for a minimum energy.

n The number of times to fit the gaus.

b The minimum width of a single bin.

C Wether this is a calibration.

w Limit the Gaussian fit to this number of standart deviations around the mean of the histogram. For energies only a lower limit is set.

W Modify the errors of the fit results to contain possible errors of the seperation variables.

f,F Function to fit to the mean/resolution values.

p,P Set parameter limits for the fit to the mean/resolution values.

q,Q Use a preset function to fit to the mean/resolution values.

y,x Set the parameters of the histograms in the first/second seperation variable.

Y,X Set different parameters for the 2-dimensional histograms in the first and second seperation variable.

G,g Set the first/second seperation variable.

z,Z Call a preset for the first and second seperation variable.

Bibliography

[An92a] J. Andruszków et al., DESY 92-066, 1992

[Ba99a] *The ZEUS forward plug calorimeter with lead-scintillator plates and WLS fiber readout*
A. Bamberger et alii, Nuclear Instruments and Methods in Physics Research A 450 (2000) 235–252, 2000

[Be34a] H. Bethe, W. Heitler, Proc. Roy. Soc. A 146 (1934) 83

[Ga89a] K.J.F. Gaemers, M. Van Der Horst, Nucl. Phys. B 316 (1989) 269; M. Van Der Horst, Nucl. Phys. B 347 (1990) 149

[Gr99a] *Studies for a new electron tagger at 6m*
R. Graciani, ZEUS note 99-038, 1999

[Gr99b] *A new electron tagger for ZEUS*
R. Graciani, ZEUS note 99-067, 1999

[Gr99c] *A new electron tagger for ZEUS*
R. Graciani, PRC, 1999

[Gr00a] R. Graciani, private correspondence

[La01a] *Untersuchung von szintillierenden Fasern für ein Spaghetti-Kalorimeter auf ihre Strahlungshärte*
N. Latuske, Diplomarbeit, University Hamburg, 2001

[Ne85a] *The EGS4 code system*
Walter R. Nelson et alii, SLAC-Report 265, 1985

[Pi93a] K. Piotrzkowski, DESY F35D-93-06, 1993

[To01a] N. Togo-Rosas, Kurarray, email to R. Wichmann, 2001

[Wi01a] R. Wichmann, private email, 2001

[Ze99a] *The Upgraded Luminosity System for the ZEUS Experiment*
ZEUS collaboration, PRC-99-09, 1999

[Ze93a] *The ZEUS detector*
ZEUS collaboration, ed. U. Holm, DESY, 1993

[Zi03a] A. Ziegler, PHD thesis in preperation

Index

background, 11, 17, 20

calibration
  border correction, 20
  central events, 18–20
  constants, 44, 47, 48
  detector, 30
  energy, 18, 30
  energy cut, 19
  first step, 18–20
  goal, 18
  incident position, 20
  max channel endpoint, 20
  prototype, 18–20
  second step, 20
  simulation, 20
  spectrum, 18, 20, 45, 46, 49–52
  trigger, 18
cell, 7, 8, 11
central cell, 13
channel, 13–15

detector, 10
  fiber, 10
  measurements, 29–40
  size, 10

e3, 14
e5, 14
eAll, 14
EGS4, 12
electromagnetic shower, 13
energy reconstruction, 14–15
  linearity, 22–23, 30–31, 37
  resolution, 14–15, 22–23, 30–33, 37–38
  spectrum, 21
  uniformity, 23–25, 33–34, 37–38
energy scan
  detector, 30–33
  prototype, 20–23

fiber, 7, 8, 10, 11, 33
  reflector, 10
  SCSF-38M, 10
  SCSF-81M, 10
fiducial volume, 14
fine scan
  detector, 33
  prototype, 23–25

gate length study, 37
  resolution, 39
geometry, 5, 7–11

high voltage, 17, 30

incident angle, 10, 11, 17, 29
incident angle study, 37
  gain, 38
  resolution, 38
incident position, 10, 17, 29

kinematic peak, 37

LED, 10
luminosity measurement, 37

photomultiplier, 7, 10, 11
photostatistic, 11, 14, 23
position reconstruction, 15–16
  basic, 15–16
  corrected, 15–16
  linearity, 15, 25–26, 33, 35
  resolution, 25, 27, 33, 36
  uniformity, 15
prototype, 10, 11
  fiber, 10
  measurements, 17–27
  size, 10
pulse shape, 39

reconstruction, 13–16

global, 13
local, 13
region, 13–15
region 3×3, 13
region 5×5, 13

sampling fluctuations, 14
shower size, 17, 18, 20
simulation, 10–11, 22–26
region, 10

testbeam
result, 27, 37–40
setup, 17–18, 29
testbeam setup, 29
trigger, 17, 29
tungsten, 7, 11
plate, 7, 9

veto counter, 17, 29

xL3, 15
xL3c, 16

ZEUS, 10, 11, 15, 16, 33, 37
MOZART, 11

Acknowledgement

First I want to thank Prof. Dr. Klaus Wick for this assignment, usefull discussions and his willingness to let me do things my way.

Building the 6m tagger was teamwork and I have only done my small share in it. Therefore I want to thank the 6m tagger group for good cooperation. The 6m tagger group consists of the members Dr. James Crittenden, Nicolas Latuske, Dr. Riko Wichmann, Andy Ziegler, Arzu Ziegler and the former members Dr. Nils Gendner and Dr. Ricardo Graciani. Especially I want to thank Dr. Riko Wichmann for reading the whole draft.

My special thanks go to Dr. Ilja Bohnet for his support, guidance and encouragement during my first year at DESY. It was a great preperation for this assignment.

I would also like to thank the members of Hamburg I group for creating a nice atmosphere and always being willing to help in case of a problem. The group consists of the members Bernd Bodmann, Rainer Peter Feller, Dr. Uwe Holm, Nicolas Latuske, Prof. Dr. Klaus Wick, Andy Ziegler, Arzu Ziegler, Thomas Zoufal and the former members Dr. Ilja Bohnet, Dr. Nils Gendner, Dr. Armin Meyer-Larsen.

Finally I would like to thank my parents Ute and Timm Krumnack for their support over all the years.

Declaration in accordance to the examination rules

I hereby state to have created this diploma thesis on my own and to have only used the facilities explicitly named.

Hiermit versichere ich, die vorliegende Arbeit selbständig angefertigt und nur die angegebenen Hilfsmittel verwendet zu haben.

(Nils Krumnack)